

Seismic Stability Against High Seismic Loads of Geosynthetic-Reinforced Soil Retaining Structures

F. Tatsuoka

Professor, Department of Civil Engineering, University of Tokyo, Tokyo, Japan

J. Koseki

Associate Professor, Institute of Industrial Science, University of Tokyo, Tokyo, Japan

M. Tateyama

Chief Research Engineer, Railway Technical Research Institute, Tokyo, Japan

Y. Munaf

Graduate Student, Department of Civil Engineering, University of Tokyo, Tokyo, Japan

K. Horii

Director, Engineering Department, Integrated Geotechnology Institute Limited, Tokyo, Japan

ABSTRACT: It is shown that there exists a big gap between the currently used design seismic coefficients $(k_h)_{design}$ for retaining walls (RWs) and the ratio of the highest peak ground accelerations to the gravitational acceleration experienced during the 1995 Hyogo-ken-nambu Earthquake. It is argued that some factors for the above include; a) the use of conservative soil strength in the design; b) positive aspects of dynamic effects arising from ductility and flexibility of RW that are not considered in the pseudo-static approaches; and c) the use of a global safety factor larger than unity. It is suggested, at the same time, that the currently used $(k_h)_{design}$ values should be increased appropriately to avoid such collapse of RWs as observed during the earthquake to a larger extent in the order of a) gravity type RWs, b) cantilever reinforced concrete RWs and c) geosynthetic-reinforced soil RWs having a full-height rigid facing. To evaluate dynamic earth pressure and failure zone size in unreinforced and reinforced backfill at high seismic loads more properly than the conventional pseudo-static methods, a modified pseudo-static approach is proposed, which takes into account the progressive process of the active failure in the backfill associated with shear banding and strain softening.

KEYWORDS: Seismic stability, Retaining walls, Pseudo-static analysis, Case histories, Model tests, Progressive failure

1. INTRODUCTION

It has been accepted that under static conditions, properly designed permanent geosynthetic-reinforced soil retaining walls (GRS-RWs) can be more cost-effective than, and can function equivalently to or even better than, conventional type retaining walls (RWs). Good performance of a number of GRS-RWs observed during a couple of recent very severe earthquakes in USA and Japan has shown that it is also the case under seismic conditions (e.g., Collin et al., 1992; White and Holtz, 1996; and Tatsuoka et al., 1996). Results obtained from recent theoretical and experimental works are consistent with the above (e.g., Bathurst and Alfalo, 1996). In this report, first some lessons from the seismic performance of representative types of RWs including GRS-RWs during the 1995 Hyogo-ken-nambu Earthquake will be summarized.

In the current aseismic design, RWs are designed to resist dynamic earth pressure, which is usually obtained by limit equilibrium-based pseudo-static stability analysis, mostly by the Mononobe-Okabe method (the original M-O method; Okabe, 1924; Mononobe and Matsuo, 1929). In such current aseismic design, conservative soil strength is

used (Table 1.1); for example, angles of internal friction, typically 35° , are assigned for cohesionless soils. These values are definitely lower than the actual peak friction angles ϕ_{peak} for such densely compacted cohesionless backfill as realized in most permanent GRS-RWs. Rather, these values are similar to the residual frictional angles ϕ_{res} for usual cohesionless soils. The use of such low design

Table 1.1 Typical soil strength values recommended for aseismic design of soil structures (Railway Technical Research Institute, 1997)

Type of backfill soil	Angle of internal friction, ϕ
1) Well graded sand, gravel and muck from hard rock	40°
2) Ordinary sand and gravel	35°
3) Poorly graded sand	30°
4) Cohesive soil*	30°

* For retaining walls not higher than 6 m and embankments not higher than 10m; cohesion is empirically replaced by shear resistance angle.

friction angles as above have been recommended for a reasonable conservatism, covering possible effects of progressive failure in the backfill and uncertainties of compaction level in each project (e.g., Bolton and Steedman, 1985; Jewell, 1991).

In the pseudo-static aseismic design methods that are employed in many countries including Japan, the design horizontal seismic coefficient $(k_h)_{design}$ for RWs is usually as low as 0.1 - 0.2. On the other hand, after having experienced very serious damage to a great number of civil engineering structures during the 1995 Hyogo-ken-nambu Earthquake, a double-level aseismic design methodology has been proposed and accepted by Japanese civil engineers (JSCE, 1996). In this method, permanent civil engineering structures are first to be designed so as to maintain their serviceability against the specified lower level seismic load (Level 1). Level 1 seismic load is equivalent to the conventional seismic design load as described above, which is considered to be equivalent to the order of 200 - 300 gals in terms of the peak (horizontal) ground acceleration (PGA). At the same time, each structure should be designed against the higher Level 2 seismic load in such that although they are allowed to exhibit some plastic deformation, they should not collapse totally and can be remedied within a short period. Level 2 seismic load is considered to be equivalent to a PGA of the order of 600 - 800 gals. Following this recommendation, a number of Japanese aseismic design specifications and codes for reinforced concrete (RC) and steel civil engineering structures have been revised. Now, RWs cannot be an exception, and it is now required to develop a rational aseismic design method for RWs including GRS-RWs to survive such very high seismic load.

When a value of $(k_h)_{design}$ equal to as high as 0.5 is employed, however, the seismic active earth pressure for cohesionless backfill obtained by the conventional pseudo-static approaches using the above-mentioned conservative friction angle becomes very high and the failure zone in the backfill becomes unrealistically very large and deep as shown later. Then, conventional type RWs as well as GRS-RWs are very difficult to be designed to have reasonable dimensions when they are to survive Level 2 seismic load. Yet, $k_h = 0.5$ is still lower than $PGA/g = 0.6 - 0.8$, which was experienced by many collapsed and uncollapsed RWs during the 1995 Hyogo-ken-nambu Earthquake (n.b., the response maximum horizontal acceleration in the RWs should have been even higher). In the second part of the paper, reasons other than the use of conservative soil strength for inconsistencies between the conventional $(k_h)_{design}$ values and the observed high PGA/g values will be discussed based on field and laboratory observations. The reasons will include positive net dynamic effects and the use of a global safety factor larger than unity.

In addition, the postulates used in the original M-O method will be examined based on field and laboratory observations and some theoretical considerations. Then, a modified pseudo-static approach to obtain reasonable design seismic active earth pressure and failure zone size for unreinforced and reinforced backfill subjected to very high seismic loads will be proposed.

Then, based on the information presented in this report, the values of $(k_h)_{design}$ for Level 2 seismic load will be tentatively suggested as a function of analysis method, design soil strength and RW type.

2. SOME LESSONS FROM THE 1995 HYOGO-KEN-NAMBU EARTHQUAKE

The major lessons obtained from the performance of RWs including GRS-RWs during the 1995 Hyogo-ken-nambu Earthquake could be summarized as follows (Tatsuoka et al., 1996). Fig. 2.1 shows the locations of the RWs referred to below.

The damaged RWs could be categorized into the following three groups;

- slightly damaged; the RW deformed and/or displaced slightly, and its reuse was soon started after some remedy work;
- moderately damaged; the RW deformed and/or displaced noticeably, but did not totally collapse, and was demolished to be re-constructed, or was substantially repaired before reuse; and
- severely damaged; the RW totally collapsed to the ground, and was demolished to be re-constructed.

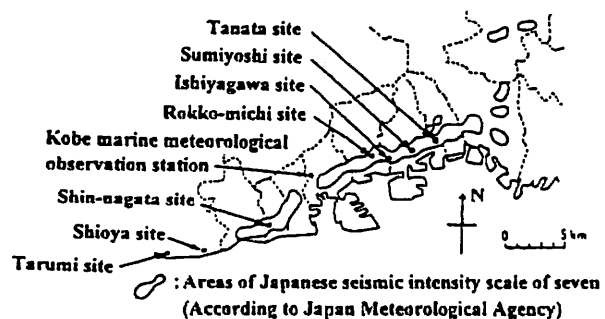


Fig. 2.1 Locations of typical soil retaining walls in Hyogo-ken-nambu referred to in the paper and Kobe Marine Meteorological Observation Station.

- The GRS-RWs having a full-height rigid (FHR) facing at Tanata was slightly damaged; the wall deformed and displaced to some extent by sliding out at its base and overturning about its base (Fig. 2.2a), but it did not show a sign of ultimate failure, despite extremely high seismic loads at the site (the estimated PGA of about 800 gals or more) and use of reinforcement layers truncated to a same short length of L/H equal to 0.56. A recently constructed

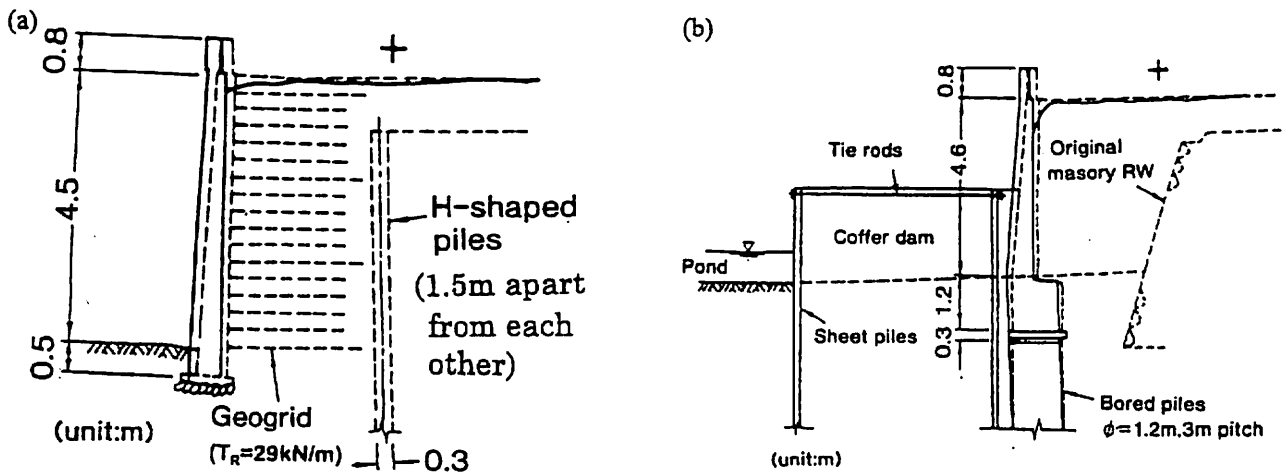


Fig. 2.2 Cross-sections before and after the earthquake of slightly damaged RWs at Tanata; a) a GRS-RW having a FHR facing (n.b., effects of the H-piles on the wall stability are considered to be very small); and b) a RC RW supported with a row of bored piles.

cantilever reinforced concrete (RC) RW supported with a row of bored piles (Fig. 2.2b), located adjacent to the Tanata GRS-RW, was also slightly damaged. Although the seismic load was less severe with an estimated PGA/g of the order of 0.5, similar GRS-RWs having a FHR facing located at Tarumi exhibited a limited amount of deformation and displacement (thus very slightly damaged). Cantilever RC RWs supported with a pile foundation constructed adjacent to these GRS-RWs

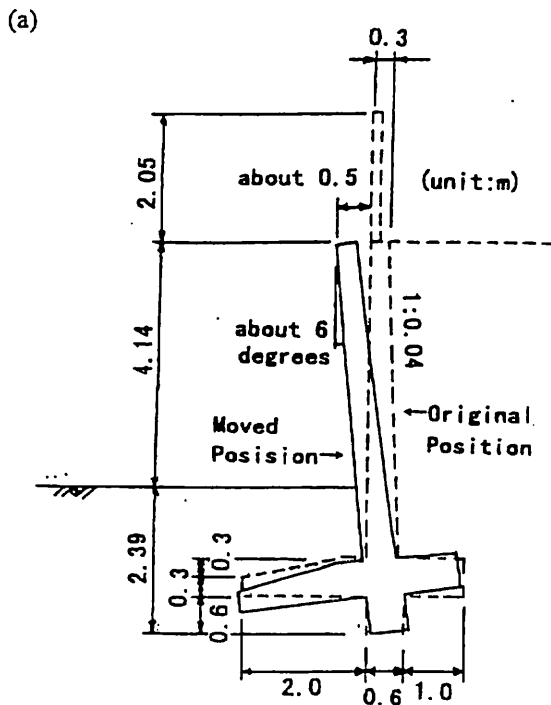
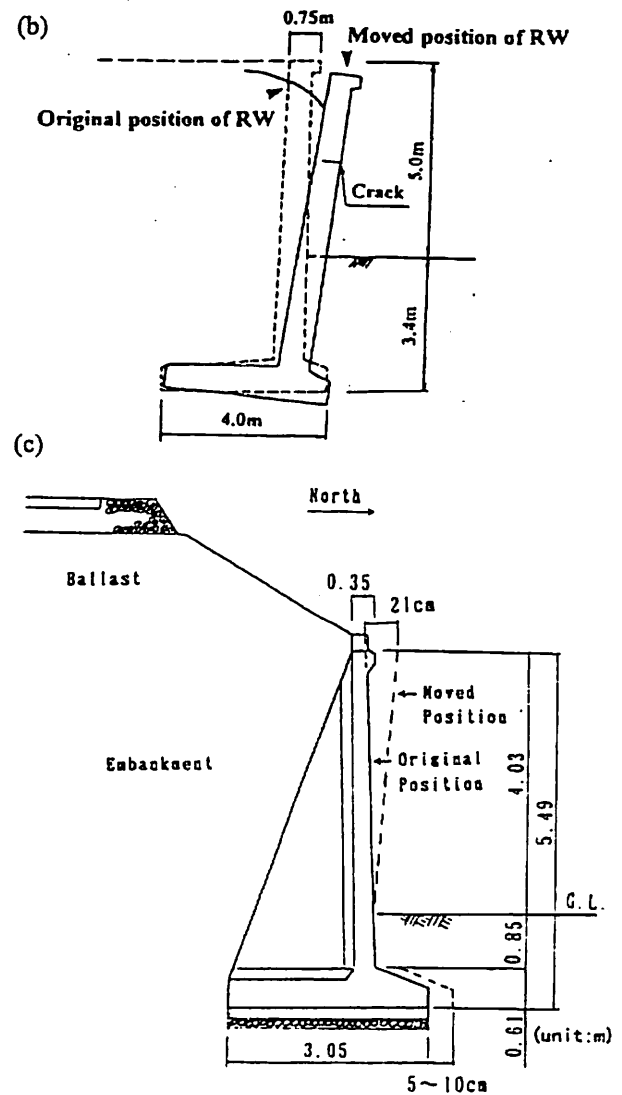


Fig. 2.3 Cross-sections before and after the earthquake of moderately damaged RWs; a) a RC retaining wall located at Rokko-michi; b) a cantilever RC RW at Ishiyagawa Station; and c) cantilever RC RW at Shioya Station



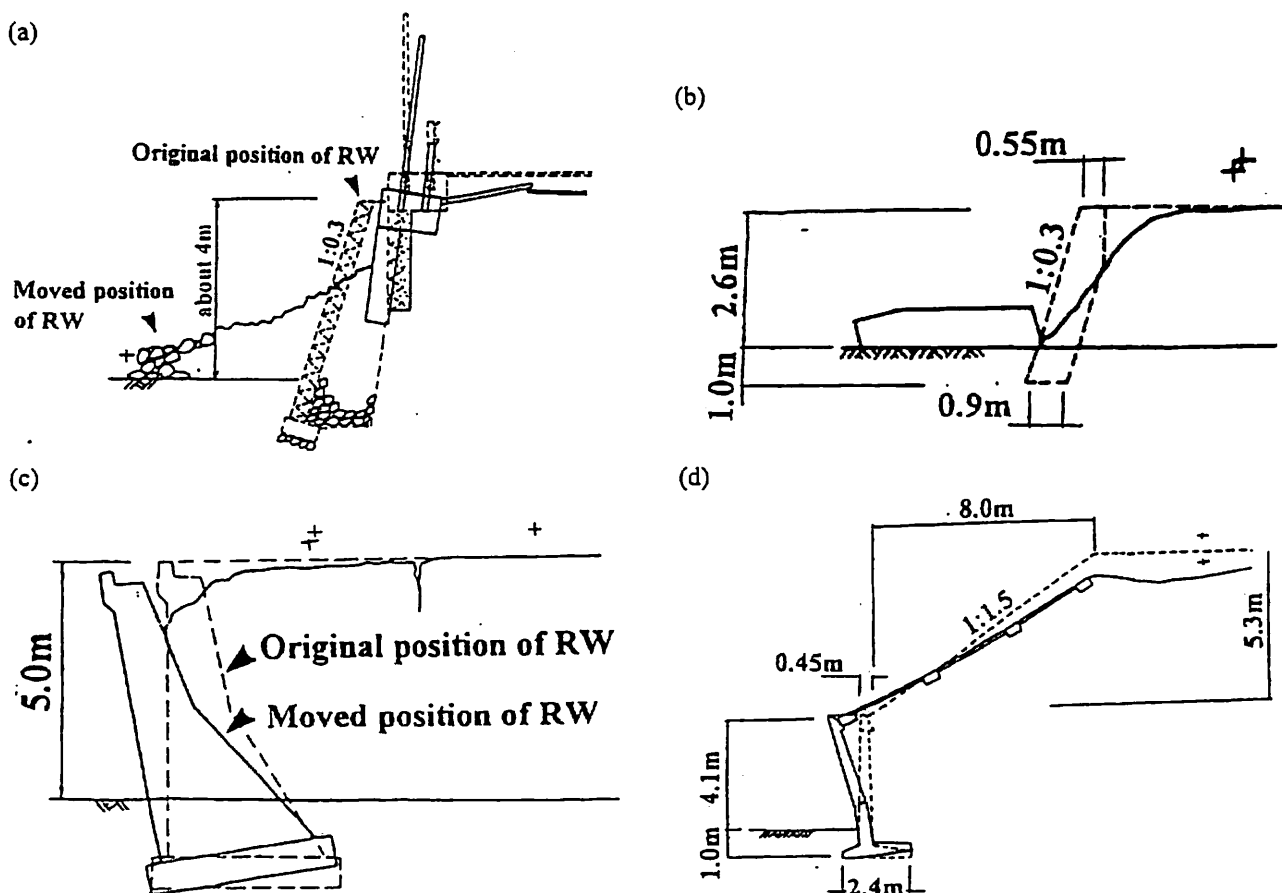


Fig. 2.4 Cross-sections before and after the earthquake of seriously damaged or totally collapsed RWs; a) a masonry RW between Setsu-motoyama and Sumiyoshi Stations; b) a leaning-type RW between Setsu-motoyama and Sumiyoshi Stations; c) a gravity-type RW at Ishiyagawa Station; and d) a poorly designed old cantilever RC RW at Shin-nagata Station

displaced similarly to the GRS-RWs. Subjected to the seismic loads similar to the Tanata GRS-RW, a reversed T-shaped cantilever RC RW at Rokko-michi (Fig. 2.3a) and those at Ishiyagawa (Fig. 2.3b) were moderately damaged. Although the seismic load was less severe, a cantilever RC RW at Shioya (Fig. 2.3c) was also moderately damaged. In comparison, a number of conventional gravity type RWs (masonry RWs and leaning type and gravity type unreinforced concrete RWs) and poorly designed old cantilever RC RWs such as that at Shin-Nagata which were located in the similarly very severely shaken areas were seriously damaged (Figs. 2.4a-d). In summary, the performance of the GRS-RWs with a FHR facing located in the severely shaken areas, particularly the one at Tanata, was satisfactory and equivalent to, or even better than, that of the recently constructed RC RWs. Reasons for these different performances should be understood.

2) The most dangerous failure mode of RW is over-turning about its bottom, because it is abrupt in a brittle and uncontrollable manner, which may result into very serious damage to structures and human beings located on the backfill and in front of the wall. A number of conventional

leaning and gravity type RWs collapsed in the overturning failure mode, triggered by large inertia force of RW and bearing capacity failure in the sub-soil below near the toe of RW, as typically seen in Figs. 2.4c and d. Sliding out of wall at the wall base is not preferable, but some amount should be admitted when subjected to very high seismic loads, because this failure mode is usually in a ductile manner, being not so abrupt as, and more stable than, the overturning failure mode. We need a relevant seismic design method for overturning at high seismic loads.

3) Fig. 2.5 shows the relationships between the safety factor and the k_h value for the Tanata GRS-RW and the RC RW at Rokko-michi obtained by the above-mentioned conventional pseudo-static design method using a design ϕ value equal to 35° for the backfill. When based on this result, the Tanata GRS-RW should have failed by base sliding at $k_h = 0.36$. Despite its good seismic behaviour, $k_h = 0.36$ is noticeably below the estimated values of PGA/g at the site (i.e., 0.8 or larger). We need an explanation for this large gap. There is a gap also for the cantilever RC RW at Rokko-michi. The gap is, however,

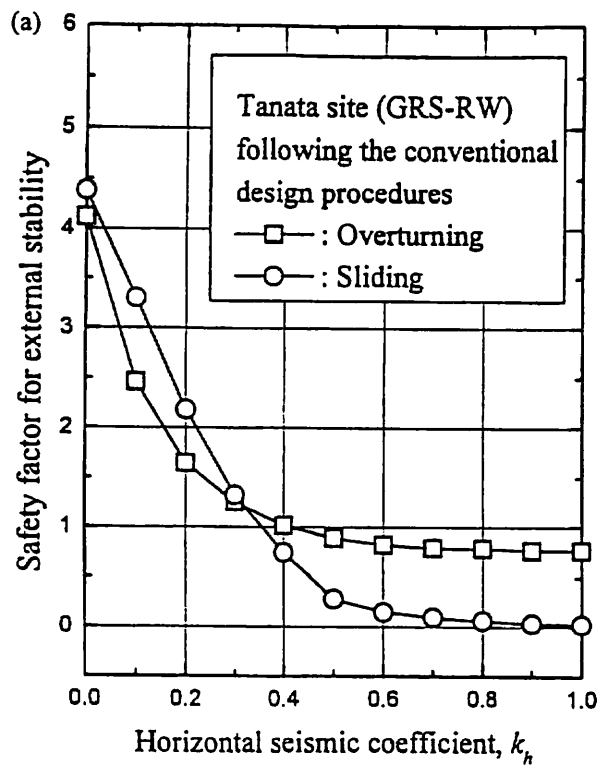
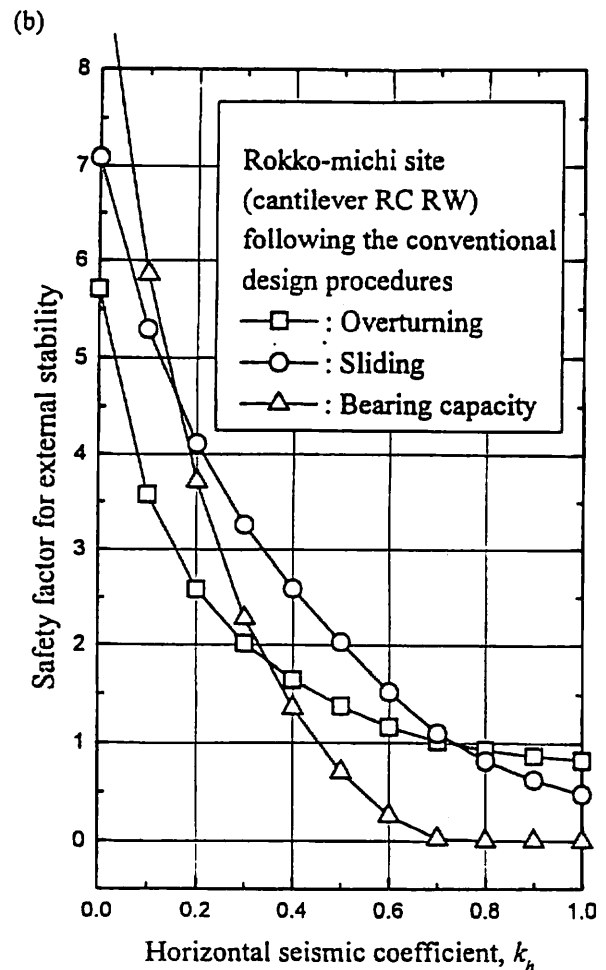


Fig. 2.5 Relationships between the safety factor and the k_h value for; a) the GRS-RW having a FHR facing at Tanata; and b) the cantilever RC RW at Rokko-michi, obtained using soil strength and simplification methods following the conventional design procedures (see Table 3.1 for calculation details).

smaller than that for the Tanata wall; the calculated critical k_h for bearing capacity failure in the sub-soil below the RW, leading to the overturning failure of RW, is higher (0.45), while the damage was severer.



4) The failure planes observed in the backfill of failed RWs, such as the gravity type unreinforced concrete RW at Ishiyagawa (Fig. 2.6a) and the leaning type unreinforced concrete RW along JR railway embankment between Setsu-motoyama and Sumiyoshi stations (Fig. 2.6b), were

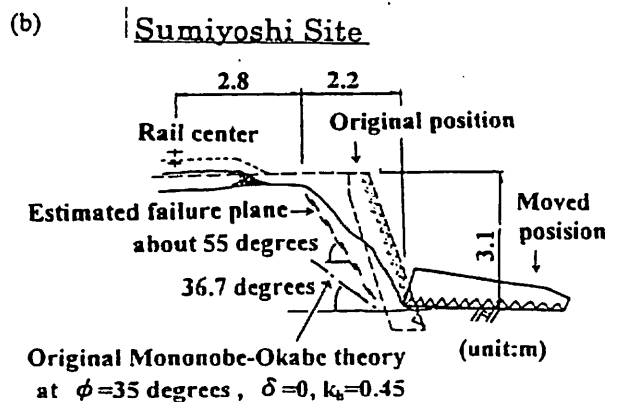
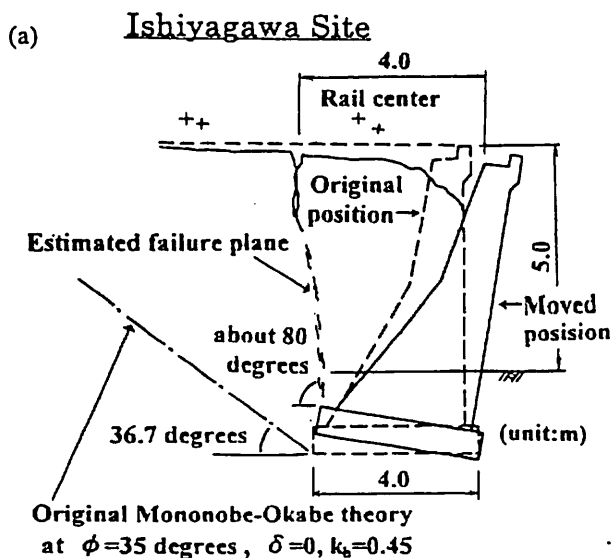


Fig. 2.6 Observed failure planes in the backfill; a) the gravity-type unreinforced concrete RW at Ishiyagawa Station; and b) the leaning-type RW along JR railway embankments between Setsu-motoyama and Sumiyoshi Stations.

much steeper than those predicted by the original M-O method using a conservative value $\phi = 35^\circ$ and based on a tentative value of k_h equal to $0.65 \cdot \text{PGA}/g = 0.65 \times 0.7 \approx 0.45$. If the reinforcement layers should be extended well back the failure zone predicted for a high design k_h value by the original M-O method using a low design soil strength, we should use extremely long reinforcement layers.

5) Effects of facing type on the deformation of reinforced soil RW were observed; subjected to seismic loads which were less severe than that for the Tanata GRS-RW, discrete panel facings of several Terre Armee RWs exhibited relatively large deformation. Due to excessive wall deformation, the upper half of one major Terre Armee wall was rebuilt after the earthquake (Tatsuoka et al., 1996).

3. EXISTING PSEUDO-STATIC APPROACHES

In most of the aseismic design specifications, codes and guidelines used in Japan for relatively important RWs, seismic active earth pressure is evaluated by the original M-O method together with the assumption of hydrostatic distribution of dynamic earth pressures (static plus dynamic components). Alternatively, the trial wedge method, which is equivalent to the original M-O method for plane backslopes, is used for backfill having an irregular backslope. As mentioned earlier, conservative soil strength is used in these aseismic design procedures, as typically listed in Table 1.1. These design soil strength values are usually not a function of the degree of compaction, resulting in no differences in calculated stability between loosely and densely compacted backfills. Rather, the required degree of compaction is specified separately, not directly linked to static and seismic stability analyses. Note again that the use of conservative soil strength does not necessarily mean that the conventional aseismic design is conservative, because of the use of conservative $(k_h)_{\text{design}}$ values.

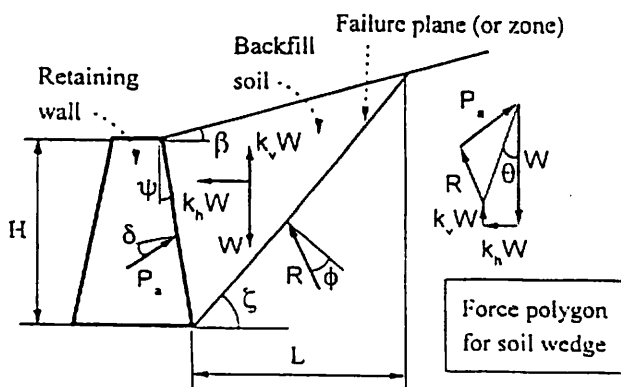


Fig. 3.1 Outline of the original Mononobe-Okabe method

In the original M-O method, the load equilibrium at the limit state (i.e., failure state) is examined for an assumed failure mechanism, and the maximum earth pressure is sought by trial and error changing the location and size of failure plane (Fig. 3.1). Fig. 3.2 shows the seismic active earth pressure coefficient $(K_a)_{\text{seismic}}$ plotted against k_h for

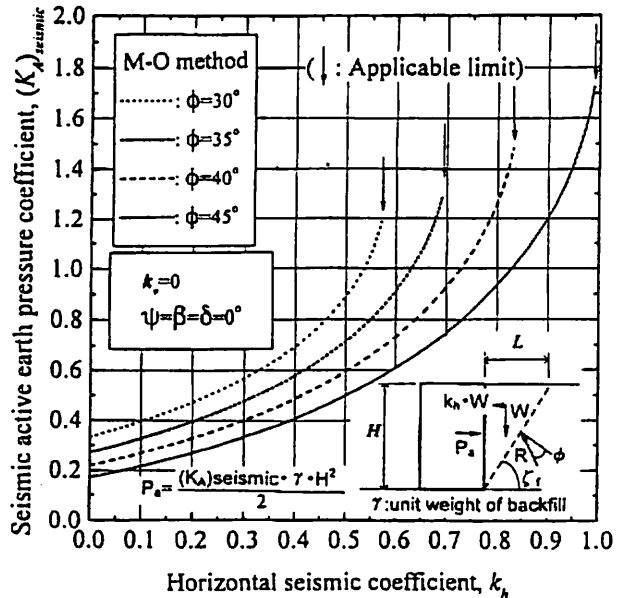


Fig. 3.2 Relationships between the seismic active earth pressure coefficient $(K_a)_{\text{seismic}}$ and the horizontal seismic coefficient k_h obtained by the M-O method for $\phi = 30, 35, 40, 45$ degrees for the simplest wall and backfill configuration.

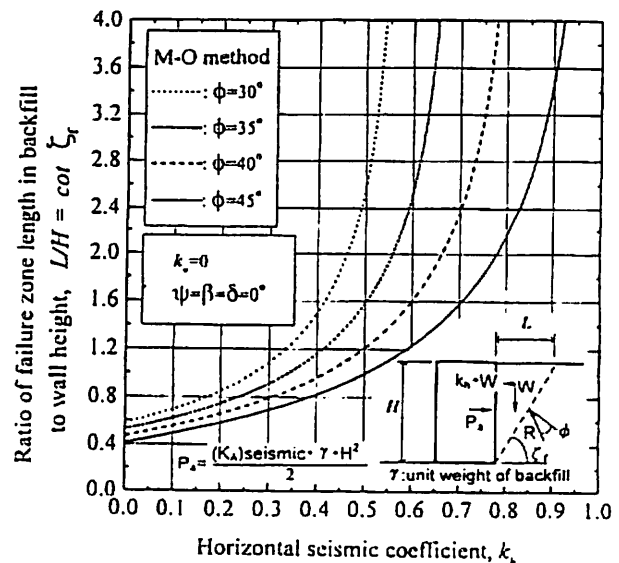


Fig. 3.3 Relationships between the size of failure zone in the backfill and the horizontal seismic coefficient k_h obtained by the M-O method for $\phi = 30, 35, 40$ degrees, corresponding to Fig. 3.2.

the simplest wall and backfill configurations as shown in the figure, obtained by the original M-O method using $\phi = 30^\circ, 35^\circ, 40^\circ$ and 45° , while Fig. 3.3 shows the size of the failure zone in the backfill. It may be seen that at a high k_h (about 0.5 or more), the use of conservative ϕ values such as 30° results into very high $(K_A)_{\text{seismic}}$ values with very deep and long failure planes.

The original M-O method is based on several postulates as summarized below:

- 1) The maximum earth pressure is obtained by changing the angle ζ of the straight failure plane starting from the heel of the wall. Therefore, the angle ζ , for the critical failure plane is a function of k_h (and k_v), and becomes smaller as the value of k_h increases.
- 2) The seismic coefficients k_h and k_v are usually applied uniformly in both vertical and lateral directions in the backfill (vertically or laterally non-uniform distributions of k_h (and k_v) are used in some modified methods as discussed below).
- 3) The friction angle ϕ is constant along the critical failure plane in homogeneous backfill. That is, the backfill soil is an isotropic and perfectly-plastic material, and the ϕ value mobilized in the failure zone is independent of the previous wall movement which has occurred before the ultimate failure of RW. This is equivalent to not considering the progressive process of active failure associated with shear banding and strain softening in the backfill.
- 4) As a result of postulates 1, 2 and 3, the distribution of dynamic earth pressure is hydrostatic with the center of gravity at one third of the wall height ($H/3$) when the backslope is level without surcharge.

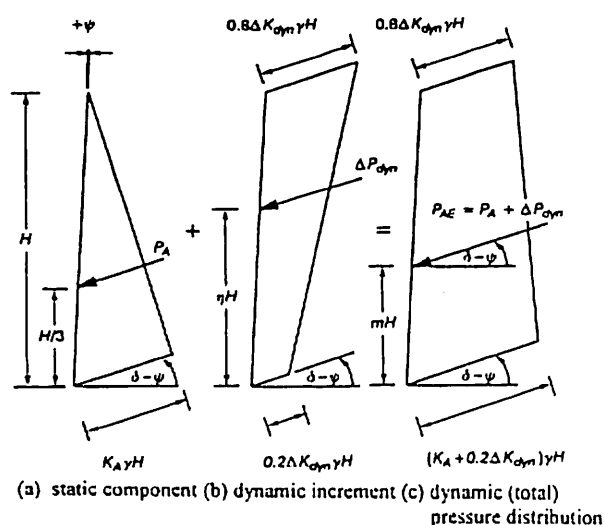


Fig. 3.4 Modified M-O method for GRS-RWs introducing a more realistic non-uniform vertical distribution of k_h (Bathurst and Cai, 1995); a) static component; b) dynamic increment; and c) dynamic (total) pressure distribution.

We should note, however, that these postulates are not relevant, as examined later in this paper in the light of the recent experimental results. For example, the postulate 3 is not relevant particularly for ductile RWs such as GRS-RWs, which can survive seismic loads largely exceeding the value at which the first active failure takes place in the backfill.

Several modifications have been proposed to alleviate some limitations of the original M-O method. The results of the previous model tests on conventional type RWs, including those by Ichihara and Matsuzawa (1973), revealed that the hydrostatic distribution assumption may be less conservative by itself. To apply to segmental GRS-RWs, Bathurst and Cai (1995) introduced a more realistic vertically non-uniform distribution of k_h (Fig. 3.4). In their method, however, a single straight failure plane starting from the heel of facing is assumed (as the original M-O method), irrespectively of the presence of reinforcement, and the reinforcement is considered to resist the seismic earth pressure obtained as above.

The two-wedge method (TW method; e.g., Jewell et al., 1984) has been used to design many GRS-RWs. This approach is particularly relevant for GRS-RWs having a FHR facing and short reinforcement (Horie et al., 1994; Fig. 3.5), since for such GRS-RWs, the failure zone consists of two wedges as observed in many model tests (Fig. 3.6a). Furthermore, the TW method can simulate single straight failure planes, thus covering the original M-O method. In the TW method, the pattern and location of failure plane is controlled by the presence of reinforcement.

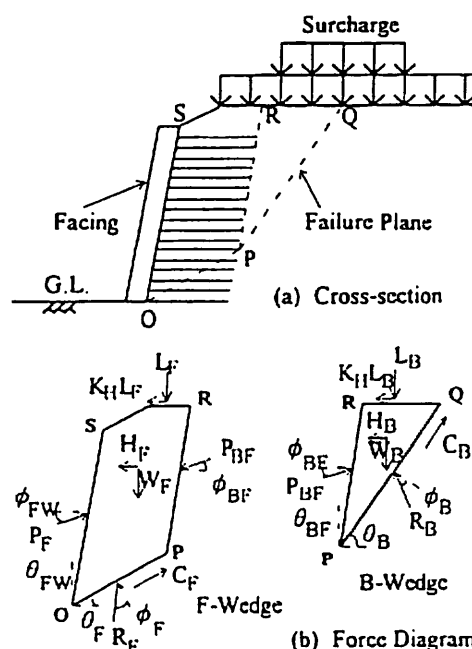


Fig. 3.5 The two-wedge method (Horie et al., 1994); a) cross-section; and b) force diagram.

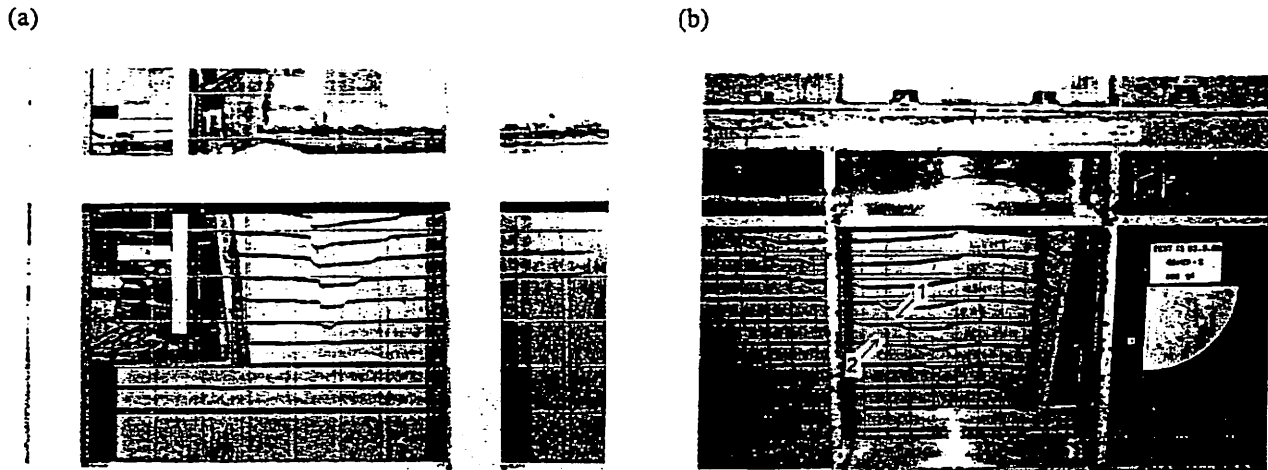


Fig. 3.6 a) Two-wedge failure mode observed in a model shaking test of GRS-RW having short reinforcements (see Fig. 4.6b and Fig. 4.7b for "Reinforced type 1"); and b) multiple failure planes observed in a model tilting test of GRS-RW having longer top reinforcement (see Fig. 4.6a and Fig. 4.7a for "Reinforced type 2") (Koseki et al., 1997).

The design procedure proposed by Leshchinsky et al. (1995) for geosynthetic-reinforced slopes and segmental walls under static loads assumes a log-spiral failure plane in the backfill. Extending the above, Ling et al. (1997) considered seismic effects by introducing a uniformly-distributed horizontal seismic coefficient C_s for the whole backfill above and below the failure plane for the tieback failure analysis (Fig. 3.7). Log-spiral failure planes cover planar failure planes as assumed in the original M-O method by setting the pole of the log spiral at infinity, but may not sufficiently model such a two-wedge failure mechanism as shown in Fig. 3.6a.

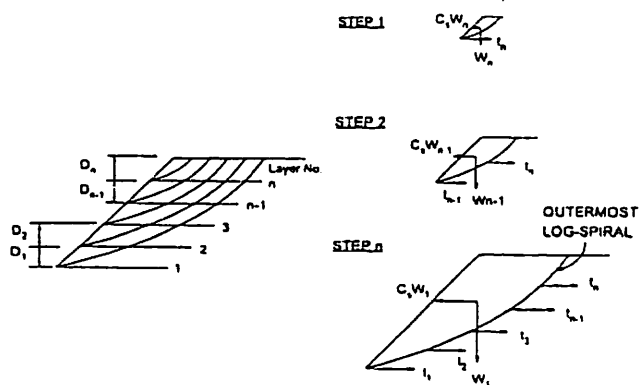
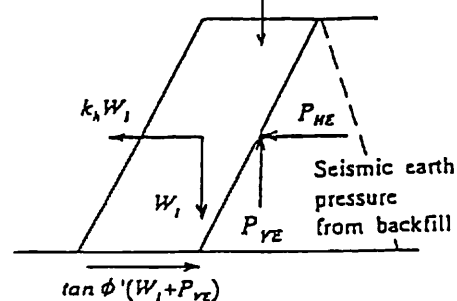


Fig. 3.7 Tie back failure analysis employing log-spiral failure plane and horizontal seismic inertia force (Ling et al., 1997).

Fukuda et al. (1994) analyzed the performance of a geogrid-reinforced slope of road embankment which survived the 1993 Kushiro-Oki Earthquake without any noticeable damage. In the aseismic design method proposed by Public Works Research Institute (1992) (Fig. 3.8a), the entire reinforced zone is regarded as a rigid body and seismic earth pressure acting from the unreinforced

backfill is evaluated by the trial wedge method or its equivalent (i.e., the original M-O method). They reported that when based on the external stability analysis described above, the safety factor of the wall against direct sliding along the wall base during the earthquake was 0.93, which is not consistent with the actual behavior. They considered that in the above method, no phase lag is introduced between the horizontal inertia force of the

(a) Reinforced zone as a pseudo-retaining wall



(b) Reinforced zone as a pseudo-retaining wall

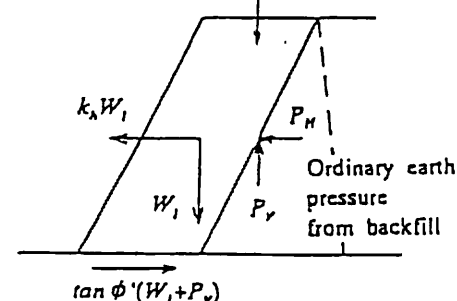


Fig. 3.8 Concept of horizontal inertia force and seismic earth pressure acting on the reinforced zone (Fukuda et al., 1994); a) when they are in the same phase; and b) when they have a phase-lag and increment of the earth pressure is zero at the maximum inertia force.

reinforced zone and the dynamic component of earth pressure acting on the back of the reinforced zone, as in many other design specifications. In order to explain this discrepancy, they assumed that the horizontal inertia force of the reinforced zone and the earth pressure acting on the back of the reinforced zone should have been out of phase. This assumption is consistent with observations in the small-scale model shaking table tests shown later. As an extreme case, they assumed that there was no dynamic component in the earth pressure when the inertia force was at its maximum, as schematically shown in Fig. 3.8b. The obtained safety factor was 1.23, which is more consistent with the actual behavior.

In the design guidelines of FHWA (1990), the value of $(k_h)_{design}$ value assigned to the reinforced part of backfill is a half of that to be applied in evaluating the seismic thrust of the earth pressure acting from the unreinforced part of backfill by considering that these two forces are unlikely to peak simultaneously. For geosynthetic-reinforced segmental RWs, Bathurst and Cai (1995) proposed a factor of 0.6, instead of 0.5.

The major limitations inherent to the pseudo-static approaches as summarized above include the following:

- 1) Deformation and displacement of RW cannot be evaluated.
- 2) The effects of dynamic effects cannot be fully nor properly accounted for, as discussed by Tatsuoka et al. (1996). The major factors of the dynamic effects include;
 - a) dynamic ductility (the capability of deforming and/or

displacing without exhibiting ultimate failure against dynamic loads exceeding the yield strength of the structure); and b) dynamic flexibility (the property which causes phase lag in a RW reducing earth pressure on the RW in a positive way while it may increase the response acceleration in a negative way). In fact, among RWs having similar seismic safety factors evaluated by the pseudo-static approach, those having a higher dynamic ductility and larger positive effects of flexibility performed better during the Hyogo-ken-nambu Earthquake (Koseki et al., 1996). Fig. 3.9 shows the $(k_h)_{critical}$ values at which the safety factor becomes unity, for the several types of conventional type RWs (Figs. 2.2b, 2.3 and 2.4) and the Tanata GRS-RW (Fig. 2.2a) evaluated by the conventional pseudo-static approaches (i.e., the original M-O method and the conventional TW method) under the following two conditions;

- A) soil strength values and wall configurations are determined following the current design procedures; the ϕ values are conservative, similar to the residual values, and passive pressure on part of the front face of underground part of RW is ignored (see Table 3.1); and
- B) peak soil strength values are used; for cohesionless soils, basically the peak friction angles estimated by relevant triaxial compression tests are used, which are larger than those described above, and the passive earth pressure on the front face of the underground part of RW is evaluated as it was at the time of the earthquake (see Table 3.2).

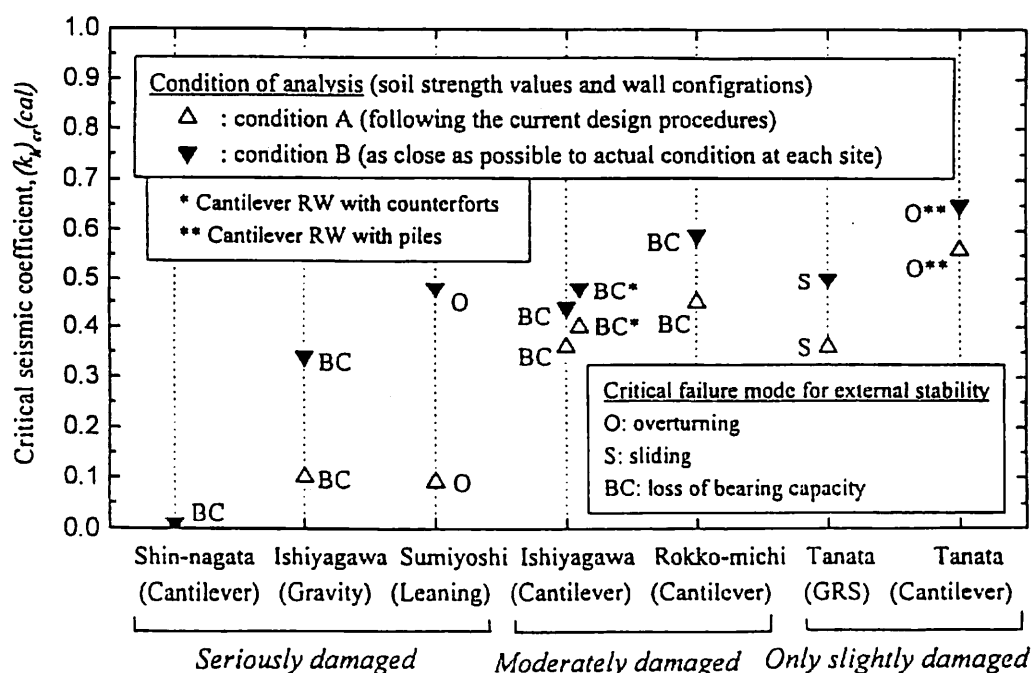
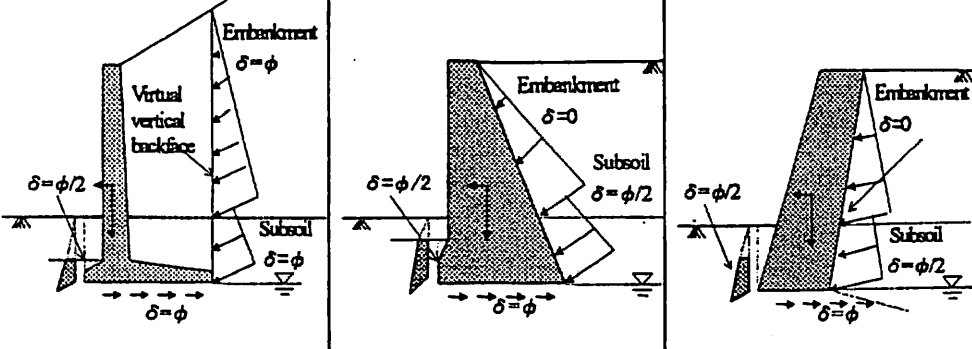
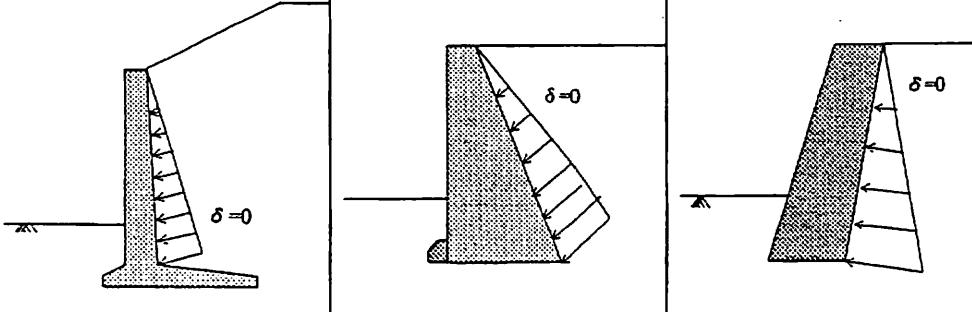


Fig. 3.9 $(k_h)_{crit}$ values for a safety factor equal to unity for ultimate failure of several conventional type RWs and the Tanata GRS-RW, evaluated by the current design methods (i.e., the original M-O method and the conventional two-wedge method) using two different soil strength values and wall configurations listed in Tables 3.1 and 3.2.

Table 3.1 Detailed calculation conditions used to obtain the $(k_h)_{\text{cal}}$ values shown in Fig. 3.9 (using soil strength values and simplification methods following the current design procedures).

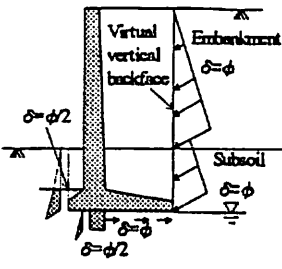
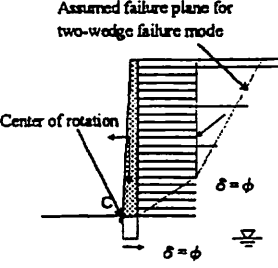
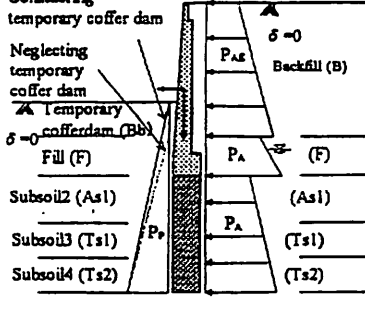
Site		Shin-nagata	Ishiyagawa	Sumiyoshi
Type of RW		Cantilever RC	Gravity**	Leaning
For external stability [condition A]	Soil property			
Active earth pressure at the back face*	γ (kN/m ³)	17.7	19.6	19.6
	C (kN/m ²)	0.0	0.0	0.0
	ϕ (°)	30.0	35.0	35.0
	δ (°)	30.0 (backfill), 30.0 (subsoil)	0.0 (backfill), 17.5 (subsoil)	0.0 (backfill), 17.5 (subsoil)
Passive earth pressure at the front face	γ (kN/m ³)	17.7	19.6	2.0
	C (kN/m ²)	0.0	0.0	0.0
	ϕ (°)	30.0	35.0	35.0
	δ (°)	15.0	17.5	17.5
Frictional resistance angle at bottom face	δ (°)	30.0	35.0	35.0
Bearing capacity of subsoil	γ (kN/m ³)	15.7	17.7	19.6
	C (kN/m ²)	49.1	0.0	0.0
	ϕ (°)	0.0	35.8	41.8

★ Surcharge was treated as equivalent backfill.

For internal stability [condition A]				
Concrete	γ (kN/m ³)	24.5	23.1 (24.5) **	23.1
	σ_c (MN/m ²)	11.8	7.7 (11.8) **	7.7
	E_c (GN/m ²)	29.9	28.3 (28.3) **	28.1
	Poisson's ratio	0.130	0.147 (0.147) **	0.177
Steel bar	σ_s (MN/m ²)	265	-(265) **	-
	A_s (cm ² /m)	19.355	-(77.6) **	-
	E_s/E_c	15	-(15) **	-

★★ For cantilever RC RW at Ishiyagawa, the same soil properties as shown for the gravity type RW at Ishiyagawa were employed except for the frictional angle at the virtual vertical backface for external stability, which was set equal to ϕ . The properties of the concrete and the steel bar employed for the internal stability analysis of the cantilever RC RW at Ishiyagawa are indicated in the parentheses at the corresponding columns for the gravity type RW at Ishiyagawa.

Table 3.1 Detailed calculation conditions used to obtain the $(k_h)_{\text{cal}}$ values shown in Fig. 3.9
(using soil strength values and simplification methods following the current design procedures). [continued]

Site		Rokko-michi	Tanata	Tanata				
Type of RW		Cantilever	Reinforced soil with FHR	Pile-supported cantilever RC				
For external stability [condition A]	Soil property			 <p>Considering temporary coffer dam Neglecting temporary coffer dam Temporary cofferdam (Bb) Fill (F) Subsoil2 (As1) Subsoil3 (Ts1) Subsoil4 (Ts2)</p> <p>Note, P_{As}: seismic active earth pressure, P_A: active earth pressure, P_P: passive earth pressure</p>				
		Active earth pressure at the back face*						
		γ (kN/m ³)	19.6	19.6				
		C (kN/m ²)	0.0	0.0				
		ϕ (°)	35.0	35.0				
		δ (°)	35.0 (backfill), 35.0 (subsoil)	0.0				
Passive earth pressure at the front face	γ (kN/m ³)	19.6	2.0	19.6	19.6	17.4	18.9	19.7
	C (kN/m ²)	0.0	0.0	0.0	0.0	0.0	0.0	0.0
	ϕ (°)	35.0	35.0	35.0	35.0	27.0	37.0	44.0
	δ (°)	17.5	35.0	0.0	0.0	0.0	0.0	0.0
Frictional resistance angle at bottom face	δ (°)	33.0 (0.0 for the front face of shear key attached to the bottom of wall)	35.0	(Bb)	(F)	(As1)	(Ts1)	(Ts2)
Bearing capacity of subsoil	γ (kN/m ³)	17.7	16.7	-	-	-	-	-
	C (kN/m ²)	0.0	0.0	-	-	-	-	-
	ϕ (°)	33.0	33.4	-	-	-	-	-

★ Surcharge was treated as equivalent backfill.

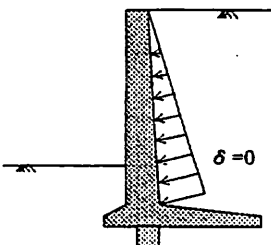
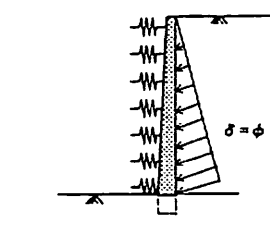
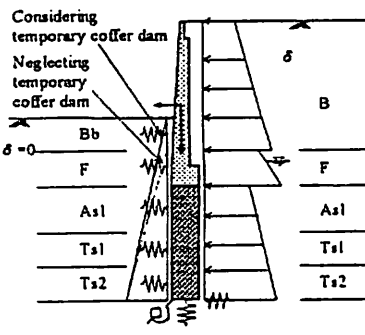
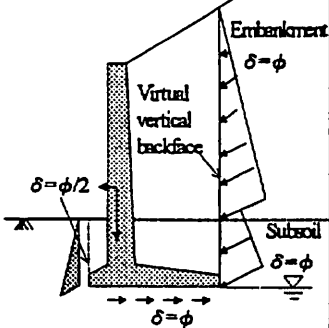
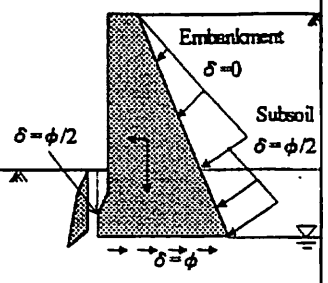
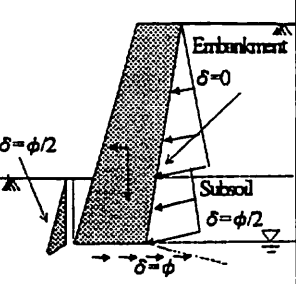
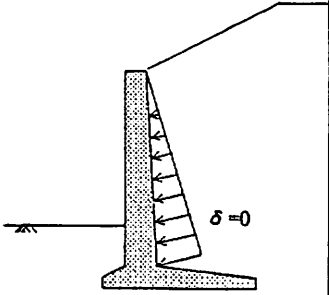
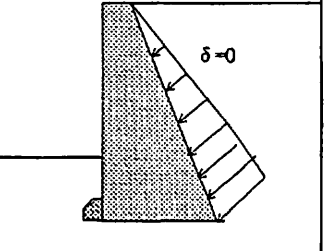
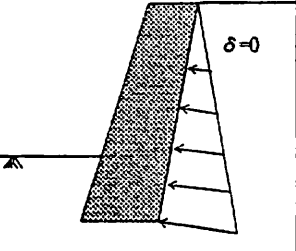
For internal stability [condition A]				 <p>Considering temporary coffer dam Neglecting temporary coffer dam Temporary cofferdam (Bb) Fill (F) Subsoil2 (As1) Subsoil3 (Ts1) Subsoil4 (Ts2)</p>				
				RC wall		Pile		
Concrete	γ (kN/m ³)	24.5	24.5	24.5	24.5	24.5	24.5	24.5
	σ_c (MN/m ²)	11.8	20.6	11.8	11.8	20.6	20.6	20.6
	E_c (GN/m ²)	82.0	24.5	23.1	23.1	23.1	23.1	23.1
	Poisson's ratio							
Steel bar	σ_s (MN/m ²)	265	481	265	265	265	265	265
	A_s (cm ² /m)	77.42	4.22	7.94	7.94	7.94	7.94	7.94
	E_s/E_c	15	15	15	15	15	15	15

Table 3.2 Detailed calculation conditions used to obtain the $(k_h)_{\text{cal}}$ values shown in Fig. 3.9
(using soil strength values and wall configurations as close as possible to those at each site)

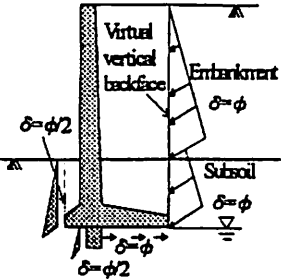
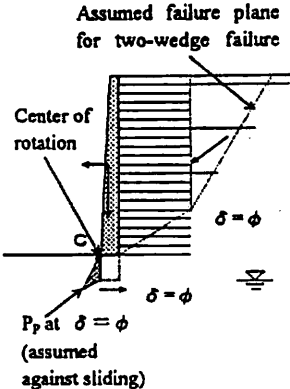
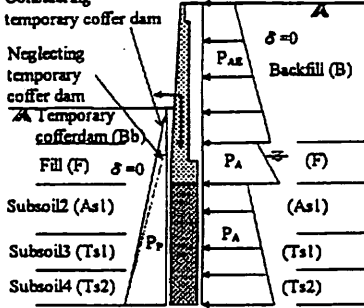
Site		Shin-nagata	Ishiyagawa	Sumiyoshi
Type of RW		Cantilever RC	Gravity**	Leaning
For external stability [condition B]	Soil property			
Active earth pressure at the back face*	γ (kN/m ³)	16.1	17.5	18.1
	C (kN/m ²)	0.0	0.0	0.0
	ϕ (°)	36.0	42.0	45.0
	δ (°)	36.0 (backfill), 36.0 (subsoil)	0.0 (backfill), 21.0 (subsoil)	0.0 (backfill), 22.5 (subsoil)
Passive earth pressure at the front face	γ (kN/m ³)	16.1	17.5	18.1
	C (kN/m ²)	0.0	0.0	0.0
	ϕ (°)	36.0	42.0	45.0
	δ (°)	18.0	21.0	22.5
Frictional resistance angle at bottom face	δ (°)	36.0	42.0	45.0
Bearing capacity of subsoil	γ (kN/m ³)	17.3	18.9	19.7
	C (kN/m ²)	49.1	0.0	0.0
	ϕ (°)	0.0	35.8	41.8

★ Surcharge was treated as equivalent backfill.

For internal stability [condition B]				
Concrete	γ (kN/m ³)	23.2	22.7 (22.5) **	23.2
	σ_c (MN/m ²)	25.8	18.8 (30.5) **	18.6
	E_c (GN/m ²)	29.9	28.3 (28.3) **	28.1
	Poisson's ratio	0.130	0.147 (0.147) **	0.177
Steel bar	σ_s (MN/m ²)	481	-(481)	-
	A_s (cm ² /m)	19.355	-(77.6)	-
	E_s/E_c	15	-(15)	-

★★ For cantilever RC RW at Ishiyagawa, the same soil properties as shown for the gravity type RW at Ishiyagawa were employed except for the frictional angle at the virtual vertical backface for external stability, which was set equal to ϕ . The properties of the concrete and the steel bar employed for the internal stability analysis of the cantilever RC RW at Ishiyagawa are indicated in the parentheses at the corresponding columns for the gravity type RW at Ishiyagawa.

Table 3.2 Detailed calculation conditions used to obtain the $(k_h)_{\alpha}(\text{cal})$ values shown in Fig. 3.9
(using soil strength values and wall configurations as close as possible to those at each site) [continued]

Site		Rokko-michi	Tanata	Tanata				
Type of RW		Cantilever	Reinforced soil with FHR	Pile-supported cantilever RC				
For external stability [condition B]	Soil property							
		Note, $P_{A\delta}$: seismic active earth pressure, P_A : active earth pressure, P_P : passive earth pressure						
Active earth pressure at the back face*	$\gamma (\text{kN/m}^3)$	18.1	16.7	16.7				
	$C (\text{kN/m}^2)$	0.0	0.0	0.0				
	$\phi (^{\circ})$	45.0	41.0	41.0				
	$\delta (^{\circ})$	45.0(backfill), 45.0(subsoil)	41.0(backfill), 41.0(subsoil)	0.0				
Passive earth pressure at the front face	$\gamma (\text{kN/m}^3)$	18.1	16.7	17.7	16.7	17.4	18.9	19.7
	$C (\text{kN/m}^2)$	0.0	0.0	0.0	0.0	0.0	0.0	0.0
	$\phi (^{\circ})$	45.0	41.0	30.0	32.0	27.0	37.0	44.0
	$\delta (^{\circ})$	22.5	41.0	0.0	0.0	0.0	0.0	0.0
Frictional resistance angle at bottom face	$\delta (^{\circ})$	33.0 (16.5 for the front face of shear key attached to the bottom of wall)	41.0	(Bb)	(F)	(As1)	(Ts1)	(Ts2)
Bearing capacity of subsoil	$\gamma (\text{kN/m}^3)$	17.9	17.4	-	-	-	-	-
	$C (\text{kN/m}^2)$	0.0	0.0	-	-	-	-	-
	$\phi (^{\circ})$	33.0	33.4	-	-	-	-	-

★ Surcharge was treated as equivalent backfill.

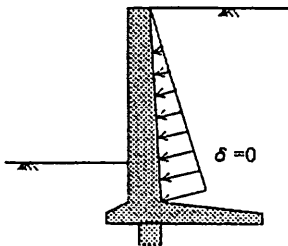
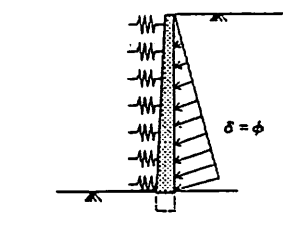
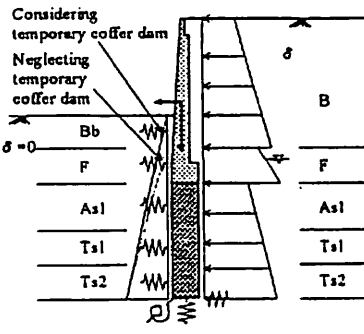
For internal stability [condition B]					
				RC wall	Pile
Concrete	γ (kN/m ³)	24.5	24.5	24.5	24.5
	σ_c (MN/m ²)	11.8	20.6	11.8	20.6
	E_c (GN/m ²)	82.0	24.5	23.1	23.1
	Poisson's ratio				
Steel bar	σ_s (MN/m ²)	265	481	265	265
	A_s (cm ² /m)	77.42	4.22	7.94	7.94
	E_s/E_c	15	15	15	15

Table 3.3 List of the $(k_h)_{cr}(\text{cal})$ values obtained following the calculation conditions listed in Tables 3.1 and 3.2.

Site	Type of RW and condition of analysis		$(k_h)_{cr}(\text{cal})$ for external stability			$(k_h)_{cr}(\text{cal})$ for internal stability			Performance during the 1995 Hyogoken-nanbu earthquake
			Overturning	Sliding	Bearing capacity	Compressive failure	Tensile failure	Shear failure	
Shin-nagata	Cantilever	A:	0.12	*	*	0.14	0.04	—	Severely damaged; very large tilting and sliding, cracking at middle height, large settlement of back slope embankment
		B:	0.24	0.16	0.01	0.40	0.23	—	
Ishiyagawa	Gravity	A:	0.25	0.64	0.10	1.97	0.47	—	Severely damaged; very large tilting, total or partial breakage at construction joints and total or very large overturning
		B:	0.63	0.78	0.34	5.20	1.14	—	
	Cantilever	A:	0.44	0.80	0.36	0.20	0.34	—	Moderately damaged; large tilting, cracking at middle height
		B:	0.89	1.23	0.44	0.80	0.78	—	
	Cantilever with counterforts	A:	0.56	0.63	0.40	0.51	0.19	—	Moderately damaged; large tilting
		B:	0.91	1.14	0.48	1.17	0.71	—	
Sumiyoshi	Leaning	A:	0.09	0.53	0.16	1.16	0.16	—	Severely damaged; complete overturning, partial breakage at ground surface level
		B:	0.48	1.06	0.49	2.23	0.77	—	
Rokko-michi	Cantilever	A:	0.72	0.73	0.45	0.52	0.68	—	Moderately damaged; large tilting
		B:	2.01	0.95	0.59	0.69	0.89	—	
Tanata	GRS	A:	0.41	0.36	—	1.29	1.22	—	Slightly damaged; slight tilting and sliding, partial minor cracking at middle height
		B:	0.60	0.50	—	1.74	1.69	—	
	Cantilever with piles**	A:	0.56	—	—	0.66 / 0.75	>1.0 / >1.0	0.99 / 0.82	Slightly damaged; slight tilting and sliding
		B:	0.65	—	—	0.77 / 0.80	>1.0 / >1.0	>1.0 / 0.92	
		A':	0.10	—	—	0.51 / 0.36	>1.0 / >1.0	0.82 / 0.24	
		B':	0.29	—	—	0.66 / 0.38	>1.0 / >1.0	0.96 / 0.32	

Condition A (upper line): using soil strength values and simplification methods following the current design procedures (refer to Table 3.1)

Condition B (lower line): using soil strength values and wall configurations as close as possible to those at each site (refer to Table 3.2)

* At Shin-nagata site, safety factors against sliding and loss of bearing capacity even at $k_h=0$ on condition A were smaller than 1.

** For cantilever RW with piles at Tanata site, internal stability analyses were conducted on both the facing and the piles, and their results are listed in the table as " $(k_h)_{cr}(\text{cal})$ for facing failure / $(k_h)_{cr}(\text{cal})$ for pile failure." Furthermore, another set of analyses was conducted by neglecting the presence of a temporary coffer dam in front of the RW, as denoted by conditions A' and B'.

Table 3.3 lists the summary of the results of the analysis with a global safety factor equal to unity. Here, the overturning failure of RW as a rigid body is assumed to occur about its toe. In actuality, overturning failure of RW may have resulted from bearing capacity failure in the subsoil below around the toe of RW, as observed with some RWs in the field (and in the laboratory as discussed later). It may be seen that when based on condition A, using conservative soil strength values, the calculated values $(k_h)_{cr}(\text{cal})$ of the two conventional gravity type (leaning and gravity types) RWs (Figs. 2.4b and 2.4c) are particularly low when compared with the others. However, for the purpose of evaluating different dynamic effects among these different RWs, the $(k_h)_{cr}(\text{cal})$ values obtained based on condition B, using more realistic soil strength values, are more informative. Then, it may be seen that except for the cantilever RC RW at Shin-nagata, these $(k_h)_{cr}(\text{cal})$ values are rather similar, despite their very different levels of damage. It is considered that positive net dynamic effects on the ultimate failure of RW may be one of the major reasons for their different seismic

behaviours. Note also that for many of the RWs (except for three cases), the $(k_h)_{cr}(\text{cal})$ based on condition A is much higher than 0.2, which is currently used for these types of RW. This difference is largely due to the use of a global safety factor, which is typically 1.5 for these types of RW.

When based on Table 3.3, the seismic stability of the pile-supported cantilever RC RW at Tanata (Fig. 2.2b) had increased largely by the presence of a temporary coffer dam in front of the RW, which was existing at the moment of the earthquake (cases A and B in Table 3.3); seemingly, the weight of the coffer dam have largely increased the overburden pressure in the sub-soil, thus have largely increased the passive earth pressure in the ground. Without these effects (cases A' and B'), the $(k_h)_{cr}(\text{cal})$ values of the RW becomes much lower, suggesting that the wall would have been damaged much more seriously than the GRS-RW at Tanata. On the other hand, the construction cost per wall length for the RC RW is about 2 - 3 times as high as that for the GRS-RW. These facts

indicate that the GRS-RW having a FHR facing could be much more cost-effective also from a viewpoint of seismic stability.

Note also that the value of $(k_h)_a$ (cal) for internal stability under condition B are similar to, or larger than, the estimated (PGA/g) values, except for an unusual case of the RC RW at Shin-nagata (see Table 3.3). Therefore, internal stability will not be discussed herein.

4. ACTIVE FAILURE PROCESS IN THE BACKFILL

4.1 Shear banding in PSC tests on sands and gravels

To examine the postulates with respect to soil properties used in the original M-O method, shear banding in granular materials will first be discussed. Densely compacted sand and gravel fails always associated with strain localization into a shear band (or shear bands) exhibiting strain softening. Therefore, the ultimate failure of the RW-backfill system is usually preceded by the active failure in the backfill associated with shear banding. Fig. 4.1 shows relationships between the shear stress level R_n and the shear deformation U_s of shear band for a variety of granular materials having a large range of particle size. These results were obtained from detailed observations of local deformation on the specimen's boundary σ_2 surface in a series of plane strain compression (PSC) tests. R_n is defined as;

$$R_n = (R - R_{res}) / (R_{peak} - R_{res}) \quad (4.1)$$

where R is the principal stress ratio σ_1/σ_3 , and R_{peak} and R_{res} are the peak and residual values of R . R_n is equal to 1.0 and 0.0 at the peak and residual states. The following important trends of behaviour have been found from Fig. 4.1 and related observations:

- In the post-peak strain softening regime, the stress level drops associated with yielding in a shear band and elastic rebound outside the shear band.
- The increment ΔU_s , by which the stress ratio drops from the peak value to the residual value is only about 5 - 10 times D_{50} for most of the granular materials (or less for Isomi gravel). This amount of shear deformation is very small when compared with the dimensions of usual full-scale RWs; for example, when the wall height H is 5 m and D_{50} is 0.2 mm, $\Delta U_s = (10 - 20)$ times D_{50} is only 0.4 - 0.8 % of H . This small figure suggests that the stress state in the shear band can become the residual state very rapidly after it develops associated with the active failure in the backfill.
- In PSC tests on sufficiently large specimens having height/width ratios larger than about 2.5 with well lubricated top and bottom ends, due to the weakening process inside the shear band, the first developed shear band further deforms without developing the second shear band(s). It would be also the case with the backfill of RW unless increasing seismic loads or backfill deformations or both change largely the principal stress directions in the backfill.

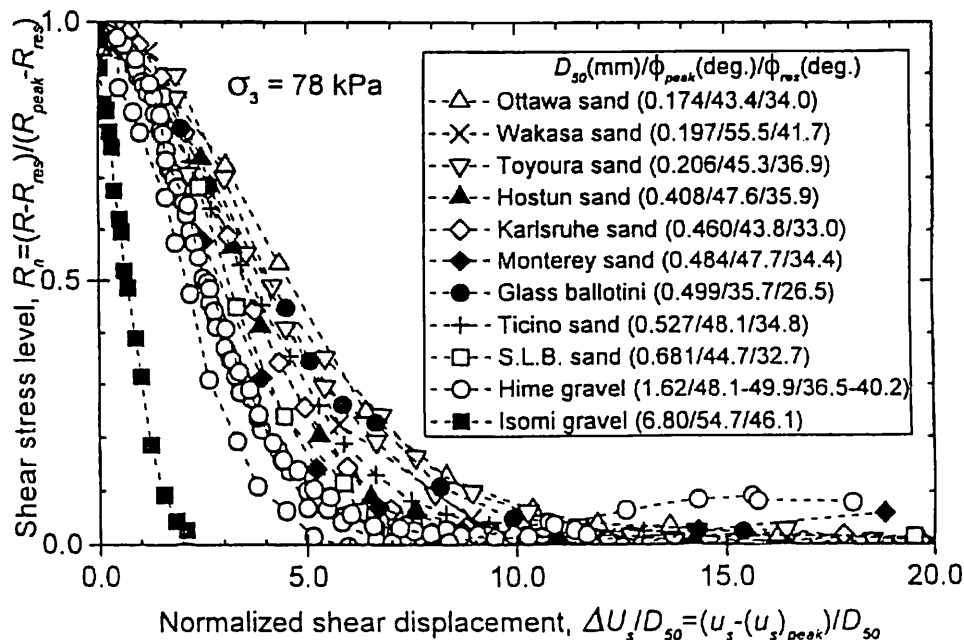


Fig. 4.1 Relationships between the shear stress level R_n and the shear deformation U_s of shear band from plane strain compression tests on a variety of granular materials with a large range of particle size (Yoshida et al., 1994; Yoshida and Tatsuoka, 1997).

These three features are relevant particularly for densely compacted backfill as that of reinforced soil RWs.

4.2 Active failure in PSE tests on sand

Yamada and Masuda (1997) performed a series of special plane strain tests in which specimens of Toyoura sand were rotated 90° after specimen preparation by air-pluviation so that the horizontal and vertical stresses σ_h and σ_v during the specimen preparation become, respectively, the axial

stress σ_a and the constant lateral stress σ_c during the plane strain tests (Fig. 4.2). The plane strain compression and extension tests were performed on specimens anisotropically consolidated at $\sigma_v/\sigma_c (= \sigma_h/\sigma_v) = 0.375$, which simulated, respectively, the passive and active failures from the K_0 condition in the backfill behind a smooth vertical RW. In the active failure test (i.e., the plane strain extension test, PSE test; Figs. 4.2c and d), the minimum earth pressure (σ_h)_{min} with ϕ_{peak} being mobilized (i.e., the active earth pressure (σ_h)_a) was

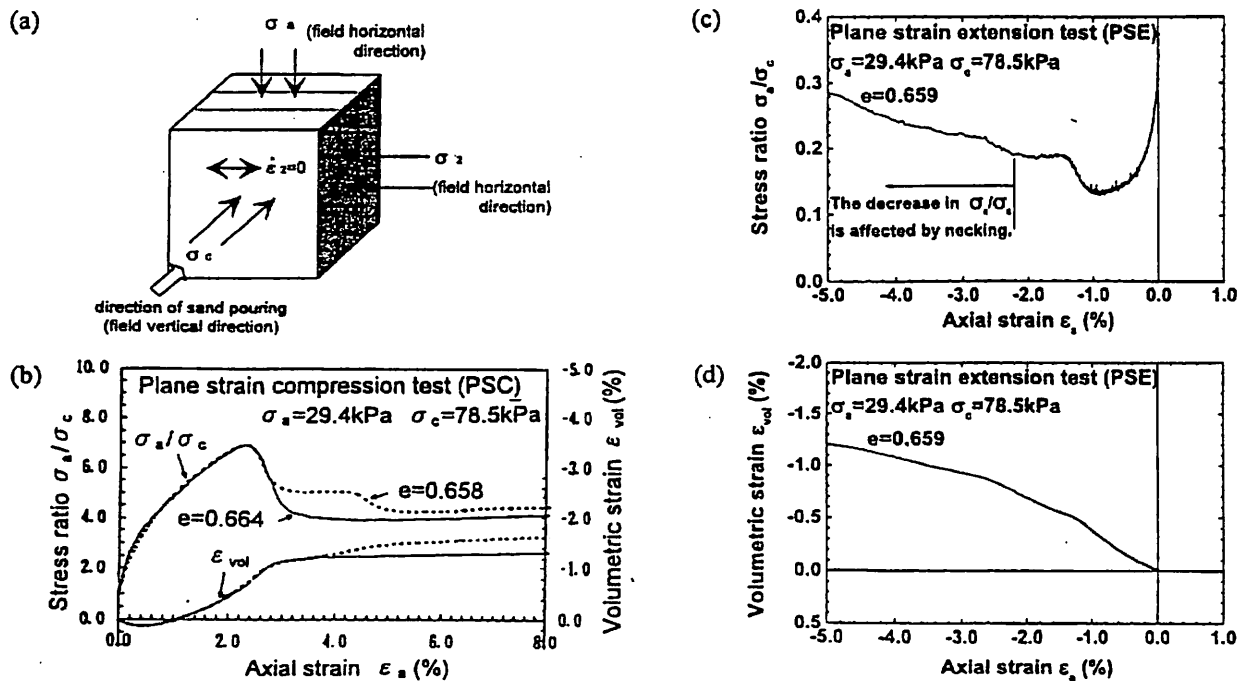


Fig. 4.2 a) Specimen configuration; and b) to d) relationships between the axial stress σ_a and the axial strain ϵ_a from monotonic active and passive tests on saturated Toyoura sand at an axial strain rate of 0.125 %/min (Yamada et al., 1996).

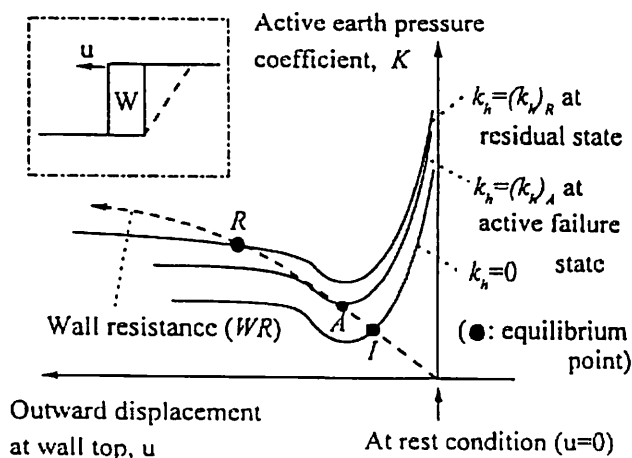


Fig. 4.3 Schematic diagram showing the active failure in the backfill and the ultimate failure of the RW.

attained at a very small axial strain of about -1.0% . The minimum earth pressure state was followed by shear banding with the axial stress σ_a (i.e., the earth pressure σ_h) increasing towards a larger value at the residual state and ϕ_{mob} decreasing from ϕ_{peak} to ϕ_{res} . The basically same process occurred in the passive failure in the PSC test (Fig. 4.2b).

It may also be inferred from Fig. 4.2c that for actual backfill soil, under static conditions or a certain seismic condition with a constant positive k_h , the pre-peak relationship between K (K_{static} or $K_{seismic}$) and u is non-linear having a negative slope dK/du , while the post-peak relationship is also non-linear but having a positive slope (see Fig. 4.3). On the other hand, at a constant u (i.e., at a constant ϕ_{mob}), the relationship between $K_{seismic}$ and k_h has a positive slope $dK_{seismic}/dk_h$. The existence of such opposite signs as shown above makes the seismic earth pressure properties very complicated and confusing.

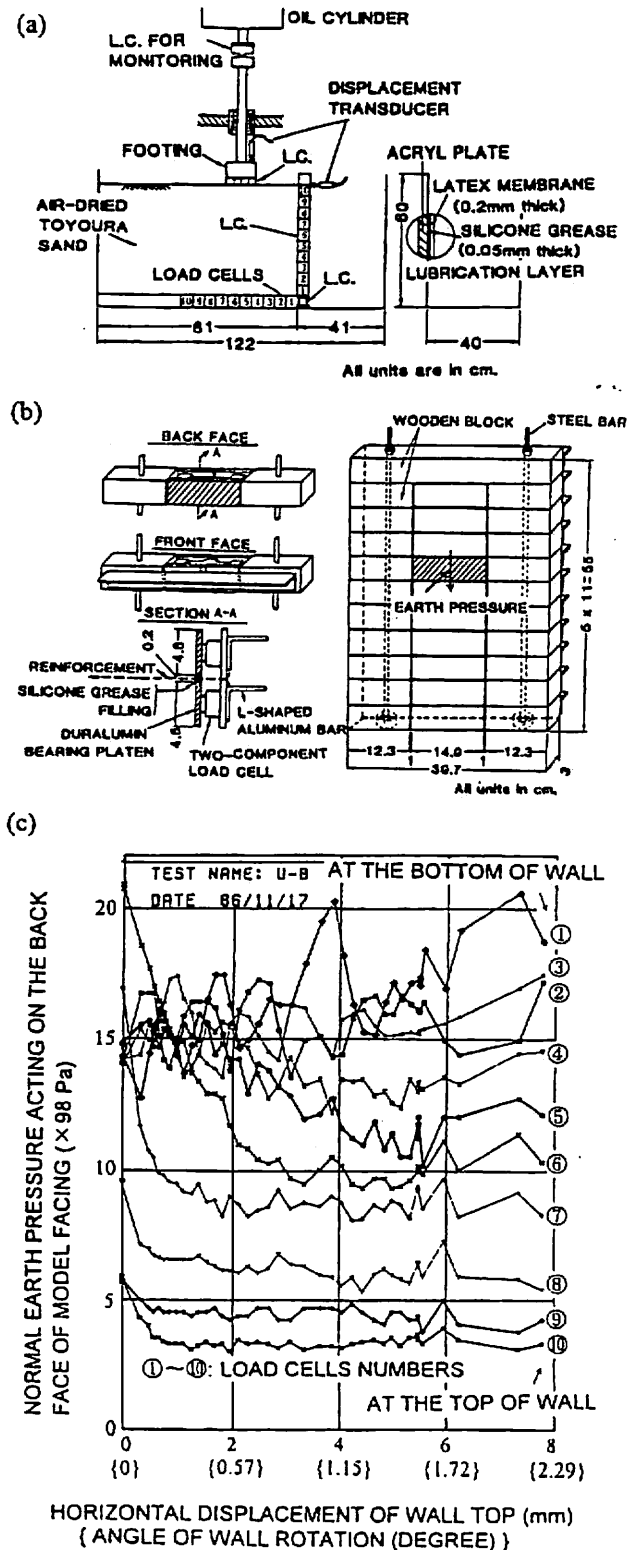


Fig. 4.4 a) Model configuration; b) details of model facing; and c) earth pressure acting on the back face of a 50 cm-high rough vertical retaining wall with backfill of air-dried Toyoura in a static model test controlling the rotation of the wall about its base (Tateyama, 1997).

4.3 Active failure in the backfill in model tests

Static model test: Tateyama (1997) measured by using ten load cells the earth pressure acting on the back face of a 50 cm-high model of rough vertical rigid RW with the backfill of air-dried Toyoura sand (Fig. 4.4). The model RW was rotated about its base at a controlled displacement rate. Similar to the above-mentioned PSE test, the minimum earth pressure was attained at a very small wall rotation (about 1.0°), which was equivalent to about -0.6 % lateral strain in the uniformly deforming active zone with $\phi = 55^\circ$. After this active failure state, at the lower part of the wall (i.e., load cell Nos. 1 to 6), the earth pressure increased associated with shear band development in the backfill. Measurements of strain field in the backfill showed that within the limit of wall rotation examined (about 2.2°), the first developed shear band further deformed without developing the second failure plane, likely due to essentially constant directions of the principal stresses in the backfill.

Shaking table tests in a centrifuge: Bolton and Steedman (1985) performed small-scale shaking tests of a 135 mm-high box RW model with the backfill of air-dried SLB sand ($D_{50} = 0.225$ mm) in a centrifuge (Fig. 4.5a). The initial centrifuging to 80 g (g denotes the gravitational acceleration) and the first earthquake loading using roughly sinusoidal cycles having the maximum amplitude of 21 % of 80 g, which was equivalent to $k_h = 0.21$, caused a total rotation of 0.57° and a total base slip of 0.39 mm of the model RW. These wall displacements were seemingly enough to initiate the active failure in the backfill. The second earthquake loading having $k_h = 0.33$ caused the ultimate failure of the RW with about a further 11 mm base slip and a visible failure plane developed in the backfill from the heel of the RW at an angle of $(90^\circ - 25.5^\circ) = 64.5^\circ$ relative to the lateral direction. It is likely that the RW exhibited ductile behaviour, surviving higher seismic loads exceeding the value that caused the active failure in the backfill. The observed angle ζ_f of the failure plane is slightly larger than the Coulomb failure angle equal to 58.4° at $k_h = 0.21$ with $\phi_{peak} = 50^\circ$ and the wall friction angle $\delta = 2/3(\phi_{peak})$ obtained by;

$$\alpha(\zeta_f) = -\tan(\phi + \delta) + \sec(\phi + \delta) \cdot \sqrt{\frac{\cos(\delta + \theta) \cdot \sin(\phi + \delta)}{\sin(\phi - \theta)}} \quad (4.2)$$

where $\theta = \tan^{-1}(k_h)$.

By using the ultimate failure seismic load $k_h = 0.33$, the failure plane angles predicted by the original M-O method using $\phi_{peak} = 50^\circ$ and $\phi_{res} = 34^\circ$ are, respectively, 52° and 36°, which are much smaller than the observed one. In a broad sense, this observation is consistent with the field behaviour (Fig. 2.6).

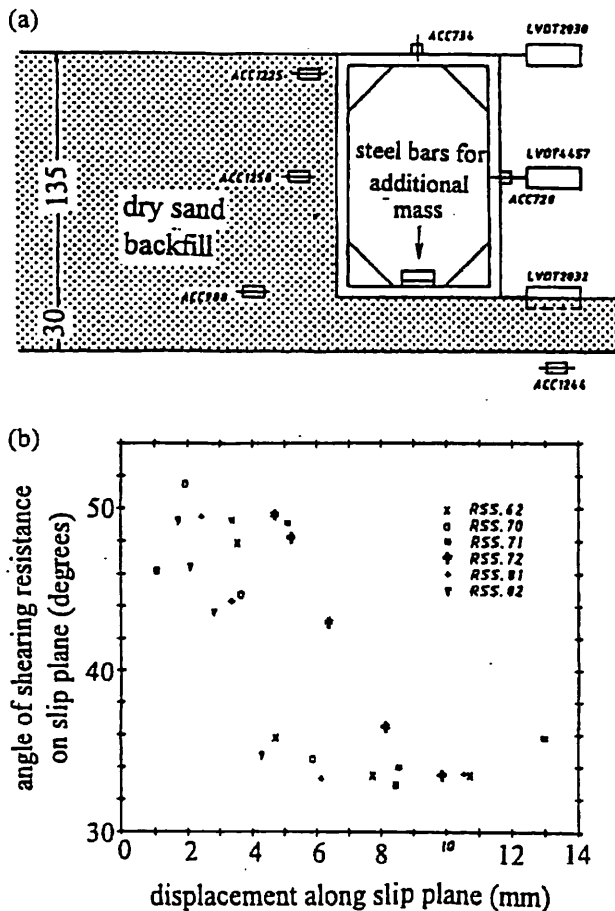
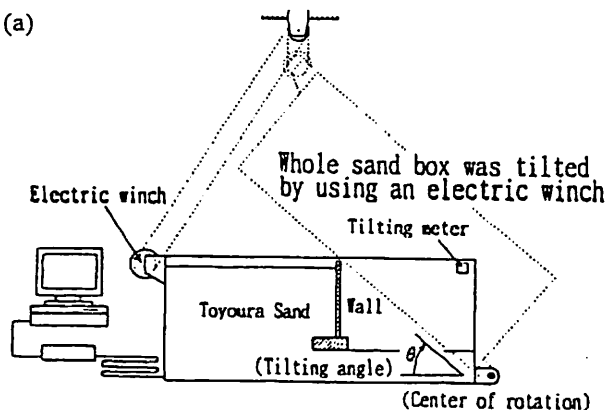


Fig. 4.5 Centrifugal shaking table tests on seismic stability of a box RW model with the backfill of air-dried SLB sand; a) test configuration (dimensions in mm); and b) relationships between the mobilized friction angle along the failure plane and the shear displacement across the shear band (Bolton and Steedman, 1985).

From the measured accelerations and displacements, the shear displacement increment across the shear band (or failure plane) ΔU , by which the stress changed from the peak value to the residual value was obtained to be about $10 \cdot D_{50}$ (Fig. 4.5b), which is very consistent with the PSC



test results shown in Fig. 4.1. It was then concluded that “10 particle diameters is such a small relative slippage in a typical situation that it might alternatively be accepted that fully softened soil strengths ϕ_{res} be invariably used on slip surfaces in sand irrespective of soil density.” This recommendation has actually been adopted in practice as discussed in INTRODUCTION. The present authors considers that this conclusion cannot be directly applied to the conventional pseudo-static approaches (e.g., the original M-O method and the conventional TW method), whereas this observation is essential for understanding and predicting better the behaviour of RWs at high seismic loads and for modifying properly the pseudo-static approaches, as discussed below.

“The seismic active failure in the backfill” and “the seismic ultimate failure of a RW” are different processes (Fig. 4.3). The seismic active failure could be defined as the mobilization of ϕ_{peak} and associated start of shear banding under seismic loading conditions, while the seismic ultimate failure of a RW occurs when the seismic earth pressure exceeds the ultimate strength of the RW, usually occurring at a wall displacement larger than that at the active failure in the backfill. Therefore, it would be appropriate to assume that ϕ_{res} is predominantly mobilized along the failure plane at the moment of the ultimate failure of RW, but not outside the failure plane (as suggested by Bolton and Steedman, 1985). This would be particularly relevant with ductile RWs, such as GRS-RWs, for which differences between the wall deformation at the seismic active failure in the backfill and that at the seismic ultimate failure of RW would be relatively large.

Tilting and shaking table model tests: Munaf et al. (1997) and Koseki et al. (1997) performed a series of small-scale static tilting tests, in which 50 cm-high models of several conventional types of RW and GRS-RWs having a FHR facing were brought to failure (Fig. 4.6a). The backfill was air-pluviated dense Toyoura sand, and each model RW was constructed on a 20 cm-thick sand layer. A model grid made of phosphor-bronze strips was

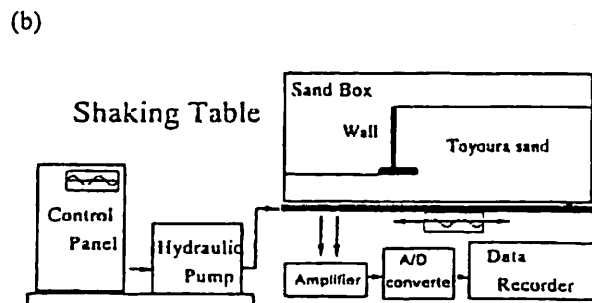


Fig. 4.6 a) Tilting tests and b) shaking table tests of cantilever-type RW model (Munaf et al., 1997).

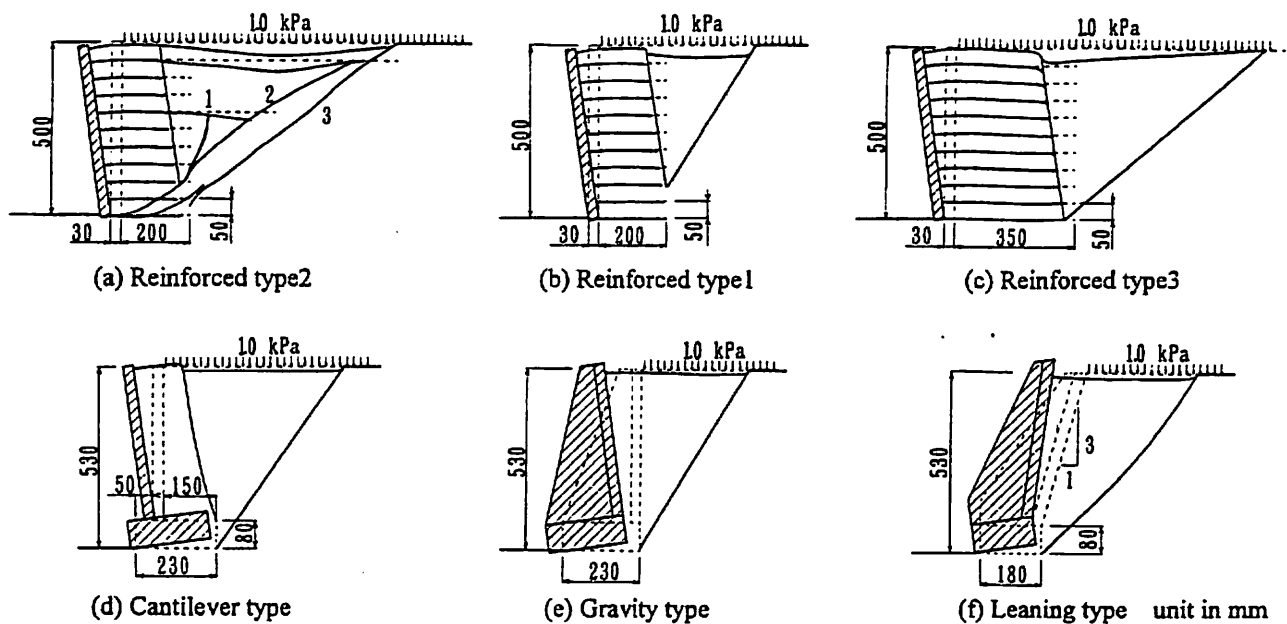


Fig. 4.7 Models of retaining walls showing their initial and displaced locations and observed failure planes; a) GRS-RW having a couple of extended top reinforcement layers, denoted as “Reinforced type 2” in Figs 4.8 and 6.2; b) GRS-RW having short reinforcement layers, denoted as “Reinforced type 1”; c) GRS-RW having moderately long reinforcement layers, denoted as “Reinforced type 3”; d) cantilever-type RW; e) gravity-type RW; and f) leaning-type RW (Koseki et al., 1997).

used to reinforce the backfill. A surcharge of 1.0 kPa, except for one test with 3.1 kPa, was applied on the backfill so as to increase the accuracy in the earth pressure measurements by increasing the pressure level in the backfill. Such static tilting model tests can simulate rather closely the stress conditions assumed in the original M-O method, except that the “vertical” stress (in the original vertical direction) decreases with tilting. In parallel, a series of shaking table tests were performed using the same RW models (Fig. 4.6b), in which the amplitude of sinusoidal waves at a frequency of 5 Hz used as input table acceleration was increased stepwise with an increment of 50 gals until the ultimate failure of RW was observed. The number of cycles at each step was about 50.

Fig. 4.7 shows the deformation of the models observed after failure in the shaking table tests. Commonly in the two series of model tests, only a single straight failure plane developed in the unreinforced backfill in back of the conventional type RWs, while a two-wedge mechanism was observed in the reinforced backfill (except for Reinforced type 2, in which multiple failure planes were observed as shown in Fig. 3.6b and 4.7a). This fact suggests that the pseudo-static approach for reinforced backfill should be different from that for unreinforced backfill such as the original M-O method. The seismic load k_h (i.e., the tilting angle or the amplitude of shaking

acceleration/g) could be increased further after the active failure plane started developing in the backfill, in particular with the reinforced soil models in the shaking table tests. However, in each test (except for Reinforced type 2), another deeper failure plane (or failure planes), which was (were) deeper than the first one, did not develop. Rather, as the k_h value increased, shear displacement was concentrated to the first developed failure plane.

Fig. 4.8 shows the relationship between the observed failure plane angle ζ_r and the observed values of k_h at ultimate failure $(k_h)_{cr(obs)}$. For the GRS-RWs, the angle ζ_r was defined for the failure plane of the back wedge developing in the unreinforced backfill behind the reinforced zone (except for Reinforced type 2). These ζ_r values have been corrected for the initial wall configurations before deformations. Each value of $(k_h)_{cr(obs)}$ was defined as the table horizontal acceleration/g or the tilting angle when a failure plane became clearly visible in the backfill and the wall displacement started increasing in an uncontrollable manner, when horizontal displacement at a wall top was about 5 % of the wall height. Note that single amplitude of the table horizontal acceleration at the active state was used to evaluate $(k_h)_{cr(obs)}$. Left-directed arrows next to some symbols mean that the respective failure plane started developing at a k_h below the $(k_h)_{cr(obs)}$. In Fig. 4.8, the theoretical relationships obtained by the original

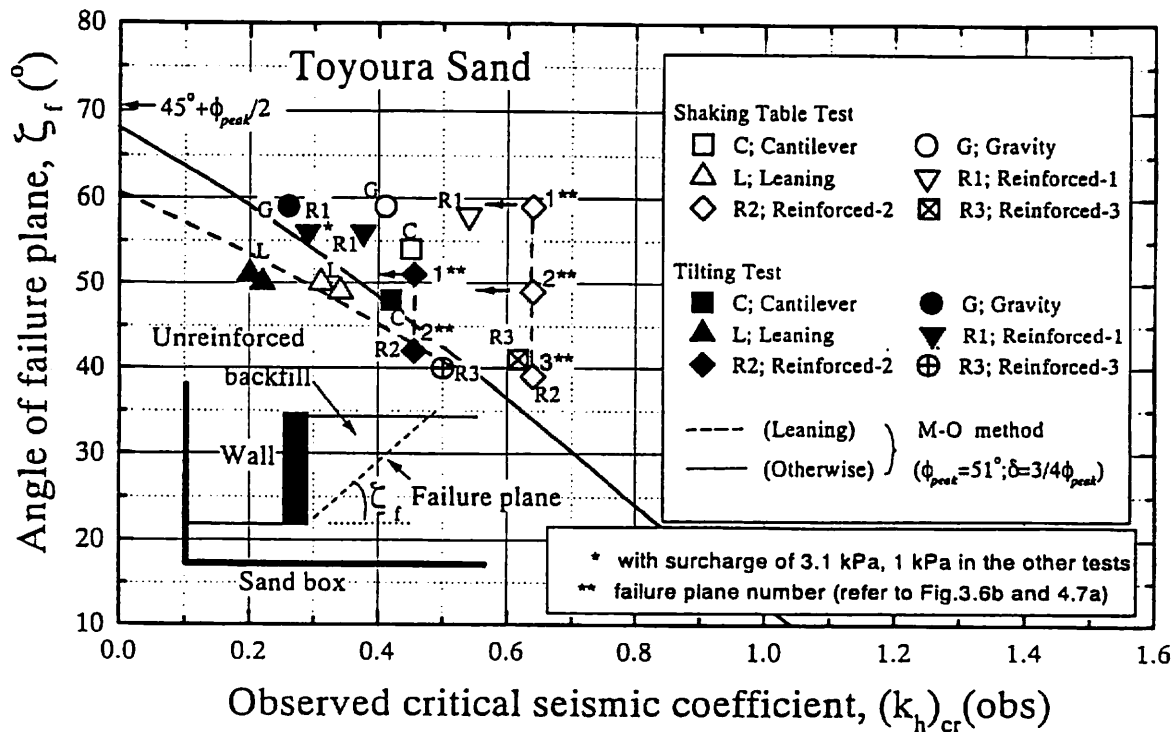


Fig. 4.8 Relationships between angle of failure plane and seismic coefficient at ultimate failure obtained from tilting and shaking table tests of model RWs (Koseki et al., 1997).

M-O method using ϕ_{peak} of the backfill equal to 51° are shown. This ϕ_{peak} value was determined based on results from PSC tests of the air-pluviated Toyoura sand used for the model tests prepared at the same density ($e = 0.644$ to 0.654) as the model tests, performed at low confining pressure ($= 9.8$ kPa) with the σ_1 direction being vertical. The frictional angle δ at the interface between the wall back face and the backfill was assumed equal to $3/4 \phi_{peak}$ ($= 38^\circ$). The ratio of $3/4$ is equal to the ratio of the angle of friction $\phi_{ss} = \arctan(\tau/\sigma)_{max}$ on the horizontal failure plane from simple shear tests to the angle of friction $\phi_{psc} = \arcsin\{(\sigma_1 - \sigma_3)/(\sigma_1 + \sigma_3)\}_{max}$ from PSC tests having the vertical σ_1 direction, both obtained for air-pluviated Toyoura sand (Tatsuoka et al., 1991). The broken curve is for the leaning type RW having an inclined back face and the solid curve is for the other conventional type RWs having a vertical back face and the GRS-RWs (except for Reinforced type 2).

The following trends of behaviour can be observed from Fig. 4.8:

- In the tilting tests, the observed relationship between ζ_f and $(k_h)_{cr}(obs)$ is generally close to the respective theoretical relationship, irrespective of RW type. It was observed that the increase in k_h which could be made after the active failure plane started developing until the ultimate failure of RW was generally small,

in particular with the leaning type RW.

- For each type of RW, the failure plane angle ζ_f is generally similar between the tilting and shaking table tests, while the $(k_h)_{cr}(obs)$ value is larger in the shaking table test than in the tilting test. The difference depends on RW type, generally larger with the GRS-RWs than the three conventional types of RWs. Furthermore, it was observed that in the shaking table tests, the k_h value could be increased from the value where the active failure plane started developing without the ultimate failure of RW to a much larger extent than in the respective tilting test, in particular with the GRS-RWs. Therefore, in the shaking table tests on these GRS-RW models, there is no clear correlation between the failure plane angle ζ_f and the $(k_h)_{cr}(obs)$ value. This result indicates that in the shaking table tests, the failure plane angle ζ_f is not totally controlled by $(k_h)_{critical}$, and the difference in the ζ_f value between the observation and the original M-O method should be explained by dynamic effects, as discussed later.

4.4 Cyclic changes in earth pressure under dynamic loading conditions

Dynamic earth pressure with an elastic backfill: Only the simplest RW configuration illustrated in Fig. 4.9 will herein be discussed. The seismic earth pressure

coefficient K_{seismic} is defined as "the total earth pressure P " / $(\gamma \cdot H^2/2)$. In general terms, the seismic earth pressure at a given moment is obtained from the equilibrium between the following two quantities;

- the earth pressure (in terms of coefficient K_{seismic}) acting on the back face of RW, which is a function of wall displacement u , being affected by seismic loads; the lateral seismic coefficient k_h is assumed to be uniformly distributed in the backfill and its positive sign is defined for the inertia force acting towards the RW; and
- the resistance against the earth pressure (in terms of K_{seismic}) of the RW supported by the subsoil, which is a function of u , being affected by the inertia force of the RW caused by the seismic coefficient $(k_h)_w$; $(k_h)_w$ may be different from k_h for the backfill.

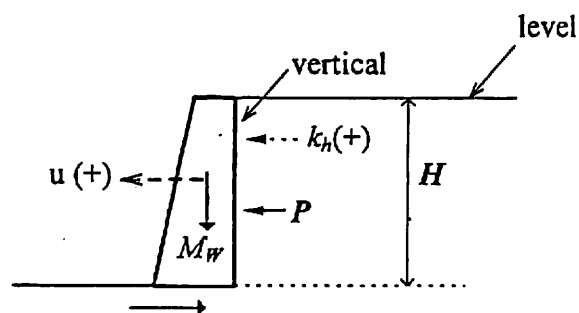


Fig. 4.9 Simple RW configuration.

Suppose that the backfill soil is a linear-elastic medium, and a rigid RW is supported linear-elastically with the subsoil (Fig. 4.10a). Suppose further that;

- the relationship between " K_{seismic} as the load applied to the RW" and u is linear with a negative slope α under static conditions or under a certain seismic condition with a constant k_h , and at a given u , the value of K_{seismic} increases proportionally with k_h ; and
- the relationship between " K_{seismic} as the resistance of the wall" and u is also linear with a positive slope β under static conditions or under a certain seismic loading condition with a constant $(k_h)_w$, and at a given u , the value of K_{seismic} decreases proportionally with $(k_h)_w$.

Equilibrium state is obtained at the intersect of the two relationships for given values of k_h and $(k_h)_w$, such as point S under the static condition and point at A at a seismic condition, Fig. 4.10a. With the values of k_h and $(k_h)_w$ cyclically changing proportionally to each other and ignoring any phase difference between them, a linear relationship between K_{seismic} and u at equilibrium is then obtained, such as ASB in Fig. 4.10a. Similar relationships under different conditions are obtained as schematically shown in Fig. 4.10b. The slope θ of the relationship is controlled by the values of α , β and the wall mass M_w among others. That is, the rate of increase in the seismic earth pressure with the increase in k_h and

$(k_h)_w$ (i.e., with the increase in u) becomes larger, or the positive slope θ becomes larger, as;

- the backfill becomes softer; i.e., the absolute value of negative α decreases;
- the subsoil becomes stiffer and the RW becomes more rigid; i.e., the slope β increases; and
- the wall mass M_w decreases.

In this case, the active seismic earth pressure is the largest value during each cycle of dynamic loading. On the other hand, the rate of increase in the seismic earth pressure with the increase in k_h and $(k_h)_w$ (i.e., with the increase in u) becomes smaller, or the positive slope θ becomes smaller, as;

- the backfill becomes more rigid; i.e., the absolute of negative value of α increases;
- the subsoil becomes softer and the RW becomes more flexible; i.e., the slope β decreases; and
- the wall mass M_w increases.

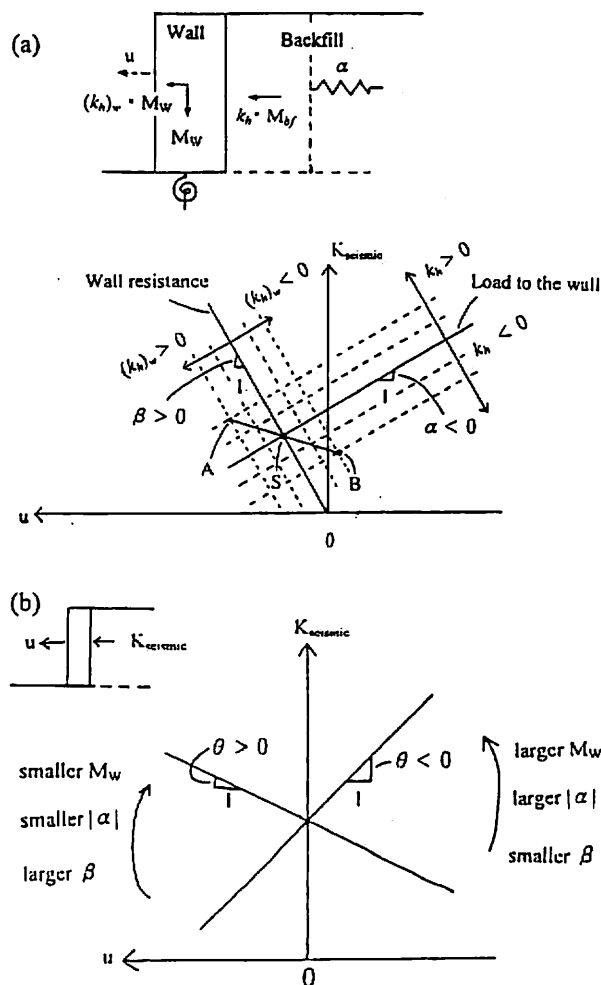


Fig. 4.10 Schematic figures showing the relationships between the dynamic earth pressure coefficient K_{seismic} and the wall displacement u with the elastic backfill and subsoil as a) the load and resistance; and b) that at the equilibrium.

In extreme cases, with the increase in k_h and $(k_h)_w$ (i.e., with the increase in u), the seismic earth pressure decreases, or the value of θ becomes negative.

Cyclic plane strain tests: Actual backfill soil and subsoil are not linear elastic. Typical hysteretic relationships between “earth pressure $\sigma_a = \sigma_h$ ” and “lateral strain $\varepsilon_a = \varepsilon_h$ ” obtained from a cyclic plane strain test on isotropically consolidated Toyoura sand are presented in Fig. 4.11 (n.b., this behaviour is close to that of a K_0 consolidated specimen under otherwise the same conditions, and see Fig. 4.2a for the specimen configuration). The results from two monotonic loading PSC and PSE tests are also plotted in Fig. 4.11 for comparison. The relationship after reversing the loading direction from a given stress state can be inferred from this result, which is essential information when interpreting the cyclically changing earth pressure acting in the backfill in shaking table tests.

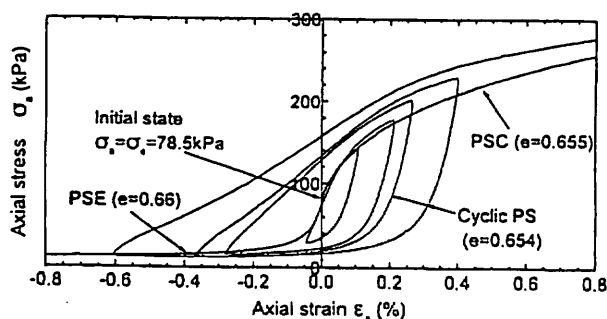


Fig. 4.11 Relationships between the axial stress σ_a and the axial strain ε_a from cyclic active and passive plane strain tests on Toyoura sand (Yamada et al., 1996).

Dynamic earth pressure in backfill:

Based on those shown in Fig. 4.10b and referring to the σ_h and ε_h relationships shown in Fig. 4.11, the relationship between $K_{seismic}$ and u in one loading cycle when the RW reaction is still linear elastic can be inferred as below. When the wall mass M_w is relatively small and the wall resistance (β) is relatively large, such a relationship as shown in Fig. 4.12a may result;

- With the increase in k_h from the static equilibrium state (point 1), $K_{seismic}$ changes to a value at the seismic active earth pressure state (point 2). Under the pre-peak condition (i.e., before the active failure in the backfill), the rate of increase in $K_{seismic}$ is decelerated by the effects of increasing ϕ_{mob} with u , and $K_{seismic}$ exhibits a relatively small change between points 1 and 2. Under the post-peak condition, on the other hand, the rate of increase in $K_{seismic}$ is accelerated by the effects of decreasing ϕ_{mob} with u , and $K_{seismic}$ exhibits a larger increase. At the residual condition, where ϕ_{mob} is independent of u , $K_{seismic}$ increases due solely to the increase in k_h .

- With the decrease in k_h from point 2, $K_{seismic}$ changes to a value at the seismic passive earth pressure state (point 3), but the change may be small due to a decrease in the earth pressure caused by the decrease in k_h .
- With the increase in k_h from point 3, $K_{seismic}$ first decreases as the earth pressure decreases at a high rate with the increase in u under the passive earth condition (see Fig. 4.11). Then, $K_{seismic}$ exhibits a relatively small change due to an increase in the earth pressure caused by the increase in k_h .

On the other hand, when the wall mass M_w is relatively large and the wall resistance (β) is relatively small, another relationship may be obtained (Fig. 4.12b);

- With the increase in k_h from point 1, $K_{seismic}$ changes to a value at the seismic active earth pressure state (point 2), but the rate of increase is smaller than it is in the case illustrated in Fig. 4.12a.
- With the decrease in k_h from point 2, $K_{seismic}$ first decreases or does not change largely due to dominant

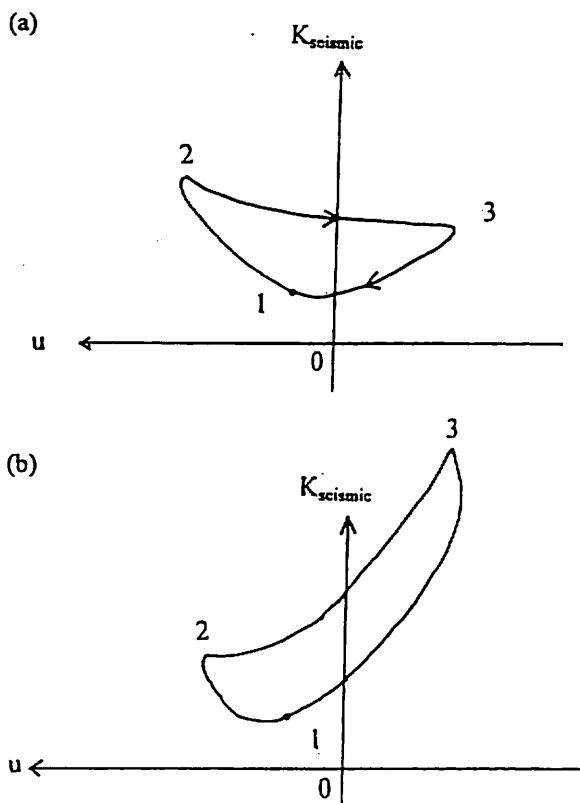


Fig. 4.12 Schematic diagrams showing the relationships between the dynamic earth pressure coefficient $K_{seismic}$ and the wall displacement u at the dynamic equilibrium; a) when the wall mass M_w is relatively small and the subsoil resistance is relatively large; and b) when the wall mass M_w is relatively large and the subsoil resistance is relatively small.

effects of decreasing k_h , but soon increases at an increasing rate of increase to the seismic passive earth pressure value (point 3) as the effects of decreasing u on the increase in $K_{seismic}$ under the passive earth condition becomes larger than those of decreasing k_h on the decrease in $K_{seismic}$.

- c) With the increase in k_h from point 3, $K_{seismic}$ first decreases at a very large rate under the passive earth condition, accelerated by large outward inertia of the wall, and then increases at a smaller rate under the active earth condition.

The above consideration suggests that the peak active earth pressure is not necessarily the largest earth pressure in each cycle; even two peaks may appear in one cycle.

Matsuo et al. (1997) measured the earth pressures acting near the back face of the facing and the back face of the geogrid-reinforced Toyoura sand backfill in a shaking table test on a 140 cm-high GRS-RW model (EH3 and EH4 in

Fig. 4.13a). As seen from Fig. 4.13b, the earth pressure EH4 has two peaks in each cycle of shaking. The relationship between the earth pressure EH4 and the table acceleration in a representative cycle is shown in Fig. 4.13c; the numbers 1 to 3 attached to the relationship correspond to those shown in Fig. 4.13b. The largest earth pressure is attained at point 3 at the passive state where the facing is moving inwards and the wall never collapses. The second largest peak, much smaller than the largest one, is attained at point 2 at the active state with the facing moving outwards. The ultimate collapse of the wall may be caused by this type of active earth pressure. The pseudo-static stability analysis for RWs deals with this

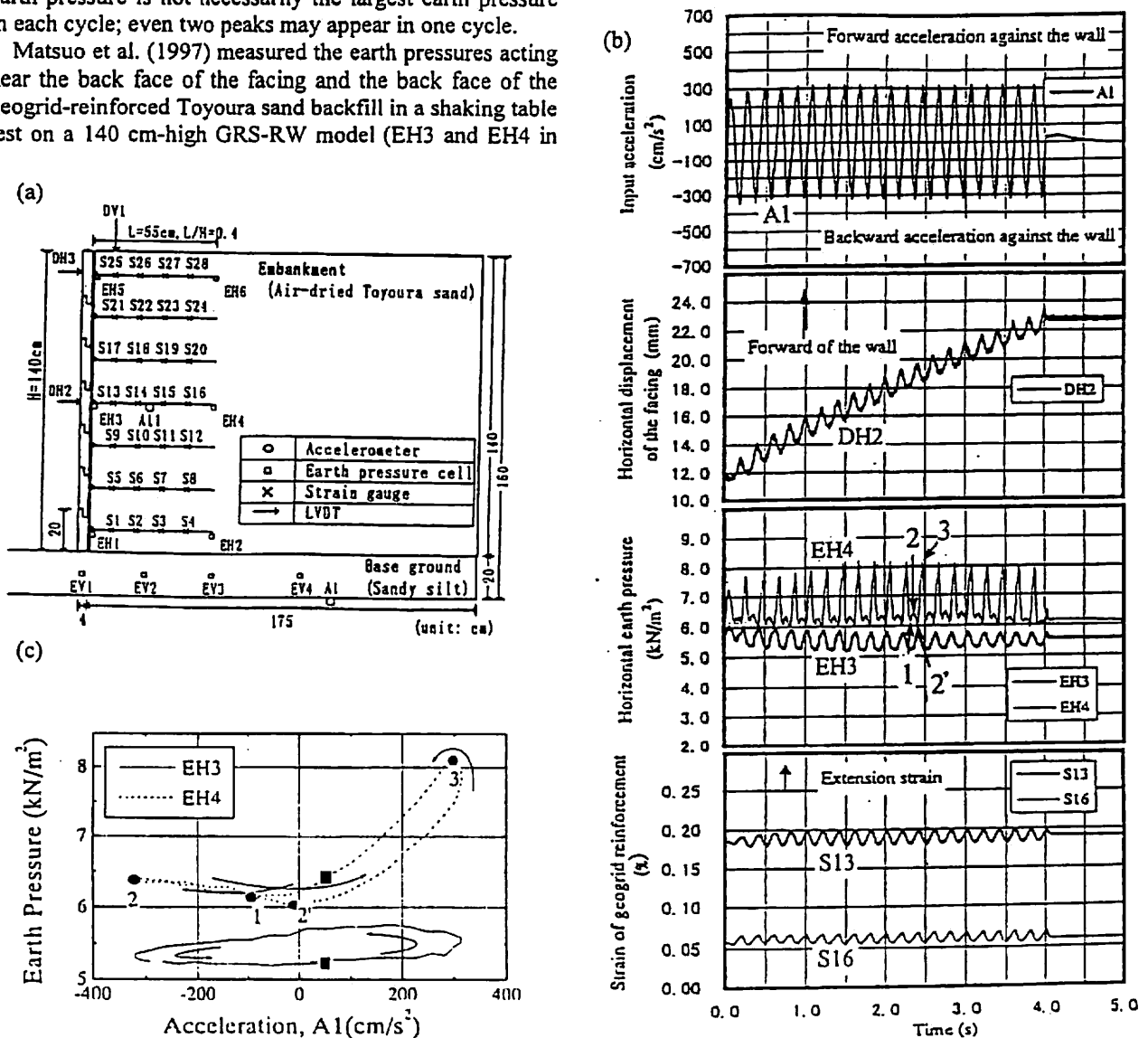


Fig. 4.13 Shaking table tests of GRS-RW model by Matsuo et al. (1997); a) test configuration for case 3; b) time histories at input acceleration of 320 gal; and c) representative hysteretic relationships between the earth pressure and the table acceleration. (A1: input acceleration; EH3 and EH4: earth pressures acting on the facing wall and the back of the reinforced soil; DH2: horizontal displacement; S13 and S16: tensile strain close to the free end and the connected end of the middle-height reinforcement.)

active earth pressure. This result shows that we should be very careful when interpreting earth pressure data from shaking table tests. In some previous cases, it seems that the largest earth pressure in one cycle was incorrectly considered as the dynamic active earth pressure.

The seismic earth pressure acting on the back face of the reinforced zone (EH4) is of the type illustrated in Fig. 4.12b for the case where the wall mass M_w is relatively large and the wall resistance is relatively low (low β). These features result from the large mass and flexibility of the massive reinforced backfill zone in the model test.

On the other hand, the earth pressure EH3 shows a very small change in each cycle, having one peak at a moment when the state was changing from passive to active (see Fig. 4.13c). It seems that due to a smaller value of β , despite a smaller value of M_w of the facing, the behaviour of EH3 became somehow different from the type illustrated in Figs. 4.12a.

There is a noticeable time lag between the moments of peak earth pressure in EH3 and EH4. This phase lag in the reinforced zone helps in increasing the seismic stability of a reinforced soil RW (i.e., part of the dynamic effects). That is, the reinforced and unreinforced zones did not act as a rigid body, and therefore, as seen from Fig. 4.13b, the active earth pressure acting on the facing could be effectively resisted by tensile forces acting in the reinforcement layers. Fukuda et al. (1994) took advantage of this feature in the seismic stability analysis of a GRS-RW (see Fig. 3.8).

5. MODIFIED PSEUDO-STATIC APPROACH FOR HIGH SEISMIC LOADS

5.1 Seismic active failure process in unreinforced backfill

The progressive process of the seismic active failure in the backfill followed by the ultimate failure of RW discussed in Chapter 4 could be summarized as shown in Fig. 5.1;

1) Stage 1: The initial static equilibrium state I is attained, controlled by many factors such as those indicated in Fig. 4.10a and other construction details such as compaction procedure of backfill. We assume that the state I is attained before reaching the active failure state A in the backfill.

2) Stage 2: With an increase in k_h from zero to $(k_h)_A$, the backfill is subjected to the process of strain hardening, approaching the active failure state A in the backfill with the minimum earth pressure (i.e., the seismic active earth pressure). The angle ζ_r of the failure plane that develops by the active failure is equal to $45^\circ + \phi_{peak}/2 - \Delta\zeta$, where the fraction $\Delta\zeta$ increases with the increase in $(k_h)_A$, while it is equal to zero when $(k_h)_A = 0.0$.

3) Stage 3: With a further increase in k_h from $(k_h)_A$ to $(k_h)_R$, the backfill is subjected to strain softening associated with shear banding, approaching the residual earth pressure state R. As discussed before, only a very small wall displacement increment Δu is needed to reach the residual state. The ϕ_{mob} values in the zones outside the shear band also decrease from ϕ_{peak} to some values, but it is by elastic rebound. The possible maximum value of ϕ_{mob} outside the shear band is still ϕ_{peak} . So, unless the seismic active earth pressure arising from the second new failure plane having ϕ_{peak} becomes larger than the earth pressure arising from the first failure plane with $\phi_{residual}$, the second failure plane does not develop and the earth pressure is controlled by the first failure plane (see Fig. 5.2).

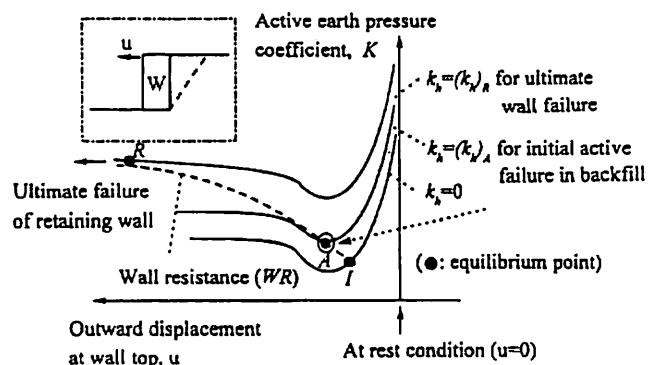
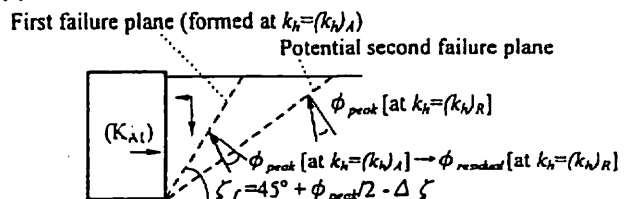


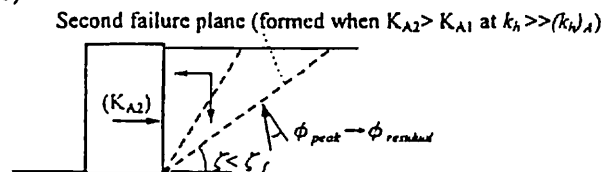
Fig. 5.1 Progressive process of mobilization of active earth pressure.

(a)



K_{A1} : earth pressure coefficient arising from fixed failure plane

(b)



K_{A2} : earth pressure coefficient arising from second failure plane

Fig. 5.2 Formation of failure planes considered in the modified method

5.2 Modified M-O method for unreinforced backfill (Koseki et al., 1997)

Usually, only a very small wall displacement u is needed for the active failure to take place in the backfill (about $0.002 - 0.003 \cdot H$). Based on this fact, it is assumed in the modified method that except for the case of a rigid RW structure supported by perfectly rigid subsoil, the seismic active failure occurs in the backfill well before the seismic ultimate failure of the RW. In the conventional pseudo-static approaches including the original M-O method, the direction of failure plane is a function of k_h for which seismic earth pressure is to be obtained with ϕ_{peak} mobilized along the failure plane. Unlike the above, it is assumed that the failure plane is fixed to the first-developed active failure plane, which is basically independent of k_h , and both ϕ_{peak} and $\phi_{residual}$ are used in the analysis. As a result, the fixed failure plane angle ζ_f is generally smaller than the one predicted by the original M-O method, the difference decreasing with the increase in k_h , $= (k_h)_A$ at which the active failure plane first develops in the backfill.

Then, the very cumbersome procedure needed in the original M-O method to obtain the maximum earth pressure becomes unnecessary. In the modified method, the value of $(K_A)_{seismic}$ is obtained by a very simple equation;

$$(K_A)_{seismic} = \left\{ \frac{[\tan(\zeta_f - \phi_{residual}) + \tan \theta] / \tan \zeta_f}{\cos(\zeta_f - \phi_{residual}) / (\cos(\zeta_f - \phi_{residual} - \delta))} \right\} \quad (5.1)$$

where $\zeta_f = 45^\circ + \phi_{peak}/2 - \Delta \zeta$;
 δ = the wall friction angle; and
 $\tan \theta = k_h$.

Basically, the value of $(k_h)_A$ should be determined by considering the deformability of RW system and other relevant factors, but it would not be simple. For practical purposes, the value of $(k_h)_A$ and the corresponding failure plane angle ζ_f may be obtained by the original M-O method using ϕ_{peak} . Then, the value of ζ_f decreases as the safety factor $(F_s)_{static}$ for the static condition increases, since the first active failure occurs at a higher $(k_h)_A$ as $(F_s)_{static}$ increases.

Fig. 5.3 compares the relationships between $(K_A)_{seismic}$ and k_h for a vertical frictionless RW with level backslope (without k_v) obtained by the following three methods;

1. the original M-O method using $\phi_{peak} = 50^\circ$;
2. the original M-O method using $\phi_{residual} = 30^\circ$; and
3. the modified M-O method when $(k_h)_A$ is equal to zero and 0.2.

In the modified M-O method, as long as using a fixed value of ζ_f irrespective of k_h , the value of $(K_A)_{seismic}$

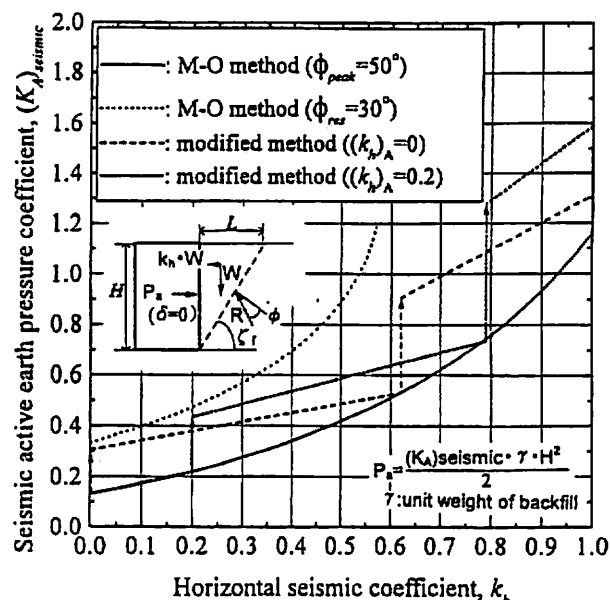


Fig. 5.3 Comparison of active earth pressure coefficient between the original and modified M-O methods for $\phi_{peak} = 50^\circ$, $\phi_{res} = 30^\circ$ and $\delta = 0^\circ$ (Koseki et al., 1997a).

increases linearly with the increase in k_h . When the k_h value becomes a certain value k_h^* , the value of $(K_A)_{seismic}$ obtained by the modified M-O method becomes the same with the value obtained by the original M-O method using ϕ_{peak} . Then, at the k_h^* value, the second deeper active failure plane is considered to develop as shown in Fig. 5.2b. The values of $(K_A)_{seismic}$ at k_h values higher than k_h^* should be obtained for the second fixed active failure plane, which becomes larger than the respective value obtained for the first active failure plane. For this reason, each relationship between $(K_A)_{seismic}$ and k_h consists of linear segments with discontinuities at the values of k_h^* . In actuality, the transition from the first active failure plane to the second one (and so on) would be somehow smooth.

The value of $(K_A)_{seismic}$ at a given k_h obtained by the modified M-O method is always equal to, or larger than, the value obtained by the original M-O method using ϕ_{peak} , while always smaller than the value obtained by the original M-O method using ϕ_{res} . Therefore, the value of $(K_A)_{seismic}$ by the modified M-O method does not become very large even at relatively high values of k_h where the values of $(K_A)_{seismic}$ by the original M-O method using ϕ_{res} become very large, or even infinite, or not possible to obtain.

Fig. 5.4 shows the relationships between the size of active failure zone, represented by $L/H = \cot \zeta_f$, and k_h , where L is the size of the failure zone on the crest of

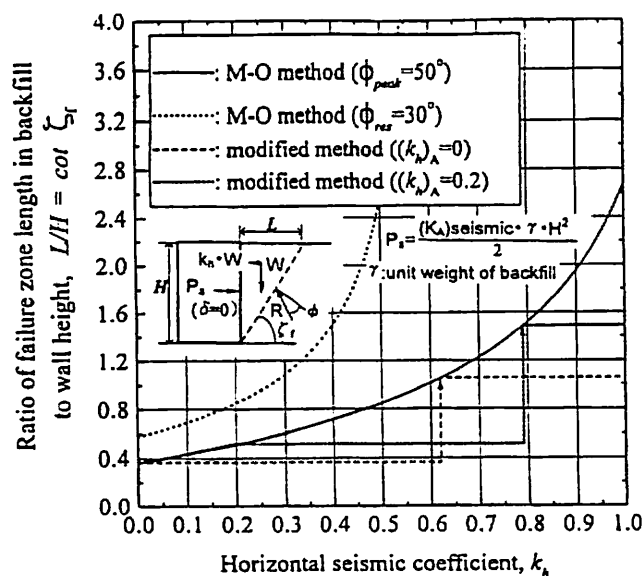


Fig. 5.4 Comparison of the ratio of failure zone length in backfill soil to wall height between the original and modified M-O methods for $\phi_{peak} = 50^\circ$, $\phi_{res} = 30^\circ$ and $\delta = 0^\circ$ (Koseki et al., 1997a).

backfill, obtained by the above-mentioned three methods. The size of the active failure zone in the backfill by the modified M-O method is always equal to or smaller than those by the original M-O method using ϕ_{peak} and always considerably smaller than those by the original M-O method using ϕ_{res} . The failure zone size by the original M-O method becomes very deep and long at very high values of k_h , particularly when using ϕ_{res} , and therefore, the relevant evaluation of the seismic stability of GRS-RWs having short reinforcement becomes very difficult. By the modified M-O method, on the other hand, realistic smaller and shallower failure planes, as observed in the Hyogo-ken-nambu Earthquake (see Fig. 2.6) and in the model tests (Fig. 4.7), are obtained.

As the modified M-O method uses both ϕ_{peak} and ϕ_{res} , it can take into account the effects of initial density of the backfill. On the other hand, in practice, their accurate evaluation would be not simple. In addition, in this method, the seismic active earth pressure is a function of $(F_s)_{static}$, which makes this method somewhat more complicated.

5.3 Modified two-wedge method for reinforced backfill

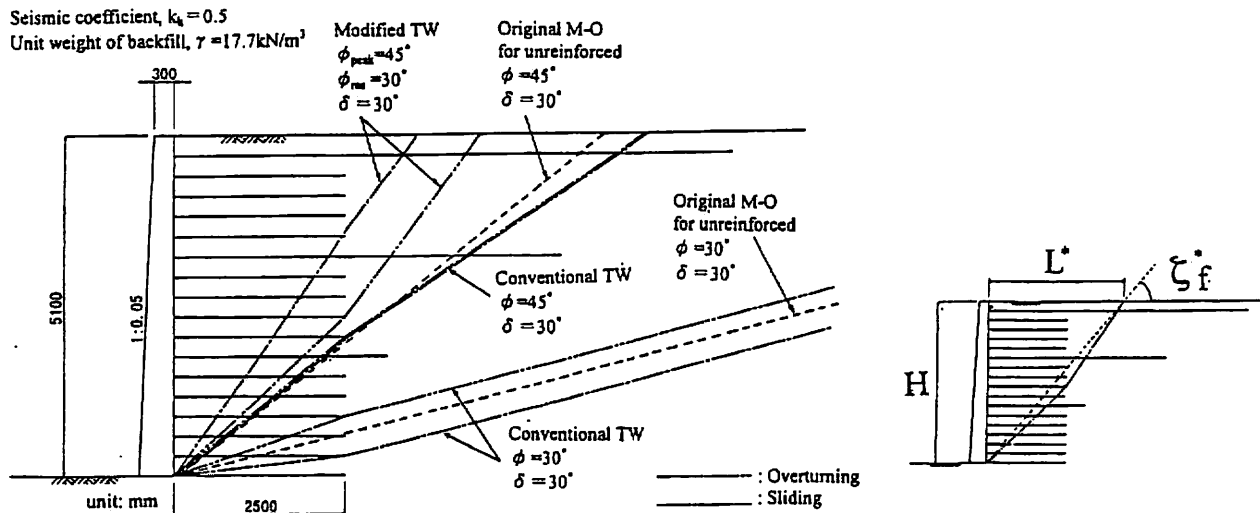
A modified two-wedge (TW) method is introduced below, in which the failure mechanism is represented by two wedges as in the conventional TW method to better simulate the seismic active failure in reinforced soil RWs,

particularly those of GRS-RWs having relatively short reinforcement. In the same way as the modified M-O method, the failure plane is basically not k_h -dependent; the first set of active failure planes with ϕ_{peak} develops at $(k_h)_A$, and the seismic earth pressures at k_h higher than $(k_h)_A$ are controlled by this first set of active failure plane with ϕ_{res} until the seismic earth pressure controlled by the second set of failure plane with ϕ_{peak} becomes larger.

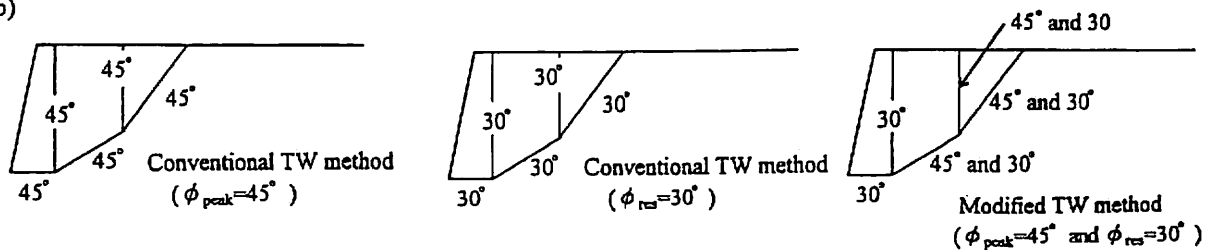
The seismic active earth pressure coefficient $(K_A)_{seismic}$ (for the earth pressure acting on the back face of FHR facing) was evaluated by the conventional TW method using either $\phi_{peak} (= 45^\circ)$ or $\phi_{res} (= 30^\circ)$ and the modified TW method using both ϕ_{peak} and ϕ_{res} for a typical configuration of GRS-RW (Fig. 5.5a), which was examined by Horii et al. (1994). The values of ϕ used in the three analysis methods are shown in Fig. 5.5b. Fig. 5.5c compares $(K_A)_{seismic}$ values when the safety factor for either overturning or sliding failure becomes the minimum. In this case, the first set of active failure plane is assumed to develop at $(k_h)_A = 0.2$. Note that this $(k_h)_A$ value was selected rather arbitrarily. Similar to those shown in Fig. 5.3, the modified method yields reasonable earth pressure, which is between those obtained by the conventional TW method using ϕ_{peak} and ϕ_{res} . According to the modified TW method, even the use of short reinforcement layers can increase substantially the seismic stability of GRS-RW at high k_h values. This feature results from the intersection of many short reinforcement layers with the potential failure planes (Fig. 5.5a).

Fig. 5.5a compares the failure planes evaluated by the different methods when $k_h = 0.5$, in which those for unreinforced backfill obtained by the original M-O method using ϕ_{peak} or ϕ_{res} are also shown for comparison. It may be seen that those for the reinforced wall evaluated by the conventional TW method using ϕ_{peak} and ϕ_{res} are similar to the respective one obtained for unreinforced backfill by the original M-O method using ϕ_{res} . On the other hand, the failure zone evaluated by the modified TW method is much smaller, being largely modified by the effects of reinforcement, despite that the reinforcement is generally short. Fig. 5.5d compares the size of the failure zone, where L' is the total length of the two wedges on the backfill crest. It may be seen that the failure zone evaluated by the modified TW method is considerably smaller, but more realistic, than those obtained by the conventional TW method.

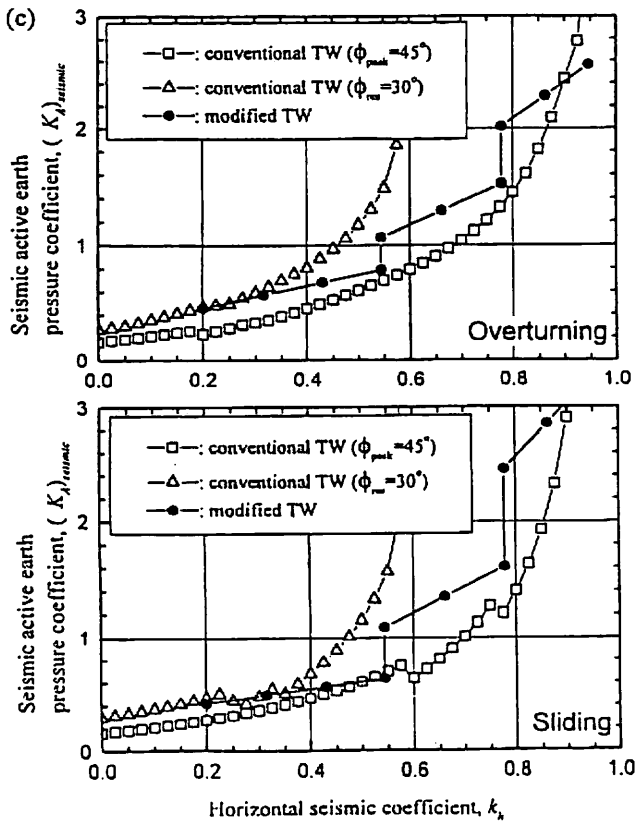
(a)



(b)



(c)



(d)

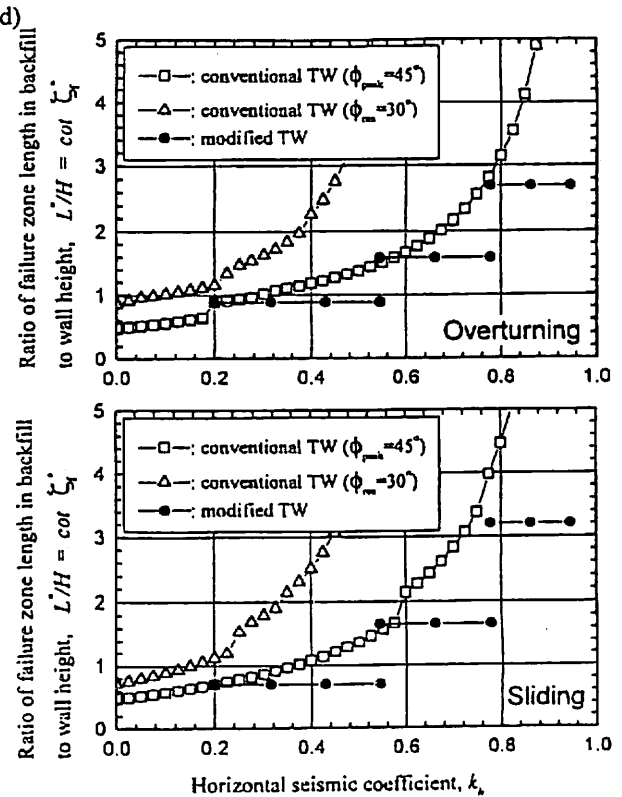


Fig. 5.5 Comparison between the conventional and modified TW methods for $(k_h)_A = 0.2$; a) wall configurations with critical failure planes; b) values of ϕ used in the analysis (the dimensions are not to scale); c) the coefficient $(K_a)_{\text{seismic}}$ of active earth pressure acting on the facing; and d) ratio of failure zone length in backfill soil to wall height.

Table 5.1 Influencing factors included in different analysis and model testing methods.

		Failure plane for ultimate failure of RW				Dynamic force					
		Location		Shape		Amplification	Non-uniform seismic force	Phase lag in the backfill	Cyclic loading effects	Randomness of cyclic loads	Inclusion of vertical component
		k_h -dependent with a constant ϕ	Fixed with ϕ_{res}	Straight	Compound						
Analysis	M-O for unreinforced backfill	Original	Yes for any k_h	No	Yes	No	No	No	No	No	Possible
		Modified	Yes for the first failure	Yes	Yes	No	No	No	No	No	Possible
	Two-wedge for reinforced backfill	Conventional	Yes for any k_h	No	Yes	Yes	No	No	No	No	Possible
		Modified	Yes for the first failure	Yes	Yes	Yes	No	No	No	No	Possible
Model tests	Tilting tests		Perhaps yes for the first failure	Perhaps yes	Yes	Yes	No	No	No	No	No
	Shaking table tests	Uniform waves	Perhaps yes for the first failure	Perhaps yes	Yes	Yes	Yes	Yes	Yes	No	Possible
		Irregular waves	Perhaps yes for the first failure	Perhaps yes	Yes	Yes	Yes	Yes	Yes	Yes	Possible
	Actual seismic loads		Perhaps yes for the first failure	Perhaps yes	Yes	Yes	Yes	Yes	Yes	Yes	Yes

Note: "Yes" does not mean that the behaviour is exactly the same with that in each specific seismic event.

5.4 Discussions on the modified pseudo-static approach

Among a number of the influencing factors for the seismic behaviour of GRS-RWs, Table 5.1 summarized the three major influencing factors; a) failure plane; b) soil strength; and c) dynamic force. It may be noted from Table 5.1 how better or poorly each analysis or model test method can simulate the actual seismic behaviour of GRS-RW. Shaking table tests using random loads could be better than those using uniform cyclic loads, and the latter could be better than pseudo-static analyses and tilting tests. It should be noted, however, that even 'yes' in this table does not necessarily mean that that particular analysis or model test method can simulate satisfactorily that factor involved in the actual behaviour of each specific GRS-RW subjected to specific seismic loads. The use in design of very sophisticated numerical analyses and model tests can be justified when nearly all the influencing factors are properly and sufficiently considered. In other words, simplified pseudo-static approaches could be still a useful engineering tool if they can reflect as better as possible the actual behaviour (such as the failure mode) and they use proper design soil strength values and seismic loads in a balanced way while taking into account the dynamic effects on the RW behaviour.

The modified TW method proposed above to evaluate seismic earth pressure in reinforced soil RWs cannot

simulate many dynamic aspects involved in the actual seismic behaviour of GRS-RWs. In particular, it is the case when it is assumed that k_h is uniformly distributed in the backfill without amplification and phase difference. Yet, the modified TW method can simulate the failure mode and earth pressure in the reinforced backfill subjected to high k_h values much better than the conventional TW method, particularly that using conservative soil strength. Similarly, the modified M-O method is more suitable for unreinforced backfill than the original M-O method.

At present, the field cases and the model tests which have been presented in this report have not been analyzed by the modified pseudo-static approach proposed above. This study is now being under way, and the results will be reported by the authors in the near future.

6. ULTIMATE FAILURE OF GRS-RWs

6.1 Ultimate failure observed in the field and model tests

Before considering a relevant aseismic design method for GRS-RWs to survive high seismic loads, observed ultimate failure of GRS-RWs will be reviewed.

Fig. 6.1 shows the relationships between the observed seismic coefficient $(k_h)_{cr(obs)}$ and the calculated values

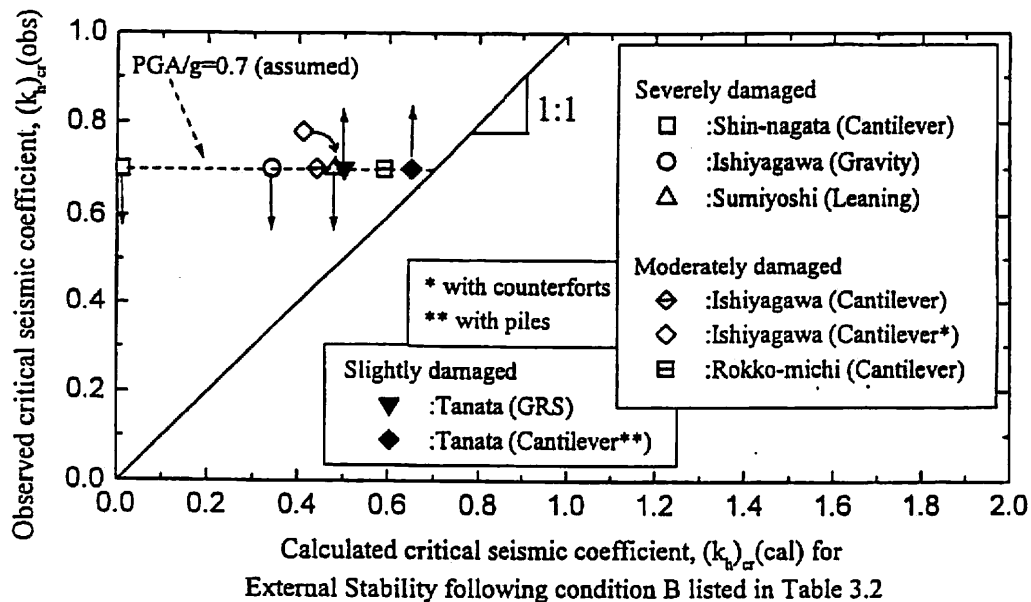


Fig. 6.1 Comparison of observed critical seismic coefficients $(k_h)_{cr}(obs)$ to calculated values $(k_h)_{cr}(cal)$ obtained following the conditions listed in Table 3.2 for RWs that experienced extra-ordinary high seismic loads during the 1995 Kobe Earthquake (Koseki et al., 1997).

$(k_h)_{cr}(cal)$ obtained by following the condition B shown in Table 3.2 (see also Table 3.3). Each $(k_h)_{cr}(obs)$ value was plotted against a common PGA/g value, which was assumed to be equal to 0.7 and the same for these RWs. The upward arrows mean that the RWs were slightly damaged, thus the actual $(k_h)_{cr}(obs)$ values for ultimate failure should be larger than the PGA/g value. The data points without arrows mean that the RWs were moderately damaged (albeit some deformation and displacement occurred), while the downward arrows mean that the RWs totally collapsed, implying that the actual $(k_h)_{cr}(obs)$ values should be smaller than the PGA/g value. This result suggests that the ratios $(k_h)_{cr}(obs)/(k_h)_{cr}(cal)$ is not the same among these RWs, which is likely to be larger in the order of; 1) the GRS-RW having a FHR facing at Tanata; 2) the cantilever RC RWs at Rokko-michi and Ishiyagawa; and 3) the gravity-type RWs at Ishiyagawa and the leaning-type RW at Sumiyoshi (particular the latter) (n.b., the cantilever RC RW at Tanata is not discussed herein, because this is not a usual case; the RW was supported by a temporary cofferdam in front of the wall at the time of the earthquake). This result suggests that the design value $(k_h)_{design}$ should be different among different types of RW; under otherwise the same conditions, the value of $(k_h)_{design}$ could be smaller for the GRS-RW.

As the amount of the field data is not sufficient, the data from the tilting and shaking table model tests, described in Figs. 4.6, 4.7 and 4.8, were analyzed. As the failure mode observed in all the tests was overturning, the results were first analyzed for this failure mode. Fig. 6.2a shows relationships between the critical seismic coefficients $(k_h)_{cr}(cal)$ yielding a safety factor of unity against overturning obtained by the original M-O method and the

conventional TW method (Horie et al., 1994) and the observed seismic coefficients $(k_h)_{cr}(obs)$. For the pseudo-static analyses, $\phi_{peak} = 51^\circ$ was used, obtained from PSC tests at $\delta = 90^\circ$ at low confining pressures using the backfill of air-dried Toyoura sand. The wall friction angle δ at the interface between the rough back face of the wall and the backfill was set $3/4 \phi (= 38^\circ)$. For the cantilever type RW, the angle of friction was set equal to ϕ_{peak} along the vertical failure plane starting from the heel of the base part of the RW. For the GRS-RWs, the bearing capacity was evaluated for the facing base having a width of 3 cm, ignoring the surcharge effects of the backfill. The allowable vertical load at the facing base was set to the bearing capacity as obtained above, then the limit equilibrium for overturning was sought. As seen from Fig. 6.2a, for many of the data points, from the tilting tests, $(k_h)_{cr}(obs)$ is much smaller than $(k_h)_{cr}(cal)$. This is likely due to;

- the effects of progressive active failure in the backfill were not considered by using $\phi_{peak} = 51^\circ$; and
- the overturning failure could have been triggered by bearing capacity failure in the subsoil, which should have taken place before the safety factor for overturning failure obtained not considering the bearing capacity failure became unity. This infer is supported by the measured earth pressure on the base of the model.

Fig. 6.2b shows relationships between whichever the smaller value of $(k_h)_{cr}(cal)$ yielding a safety factor of unity, against either overturning or bearing capacity failure, obtained by the original M-O method and the conventional TW method using ϕ_{peak} and the observed seismic

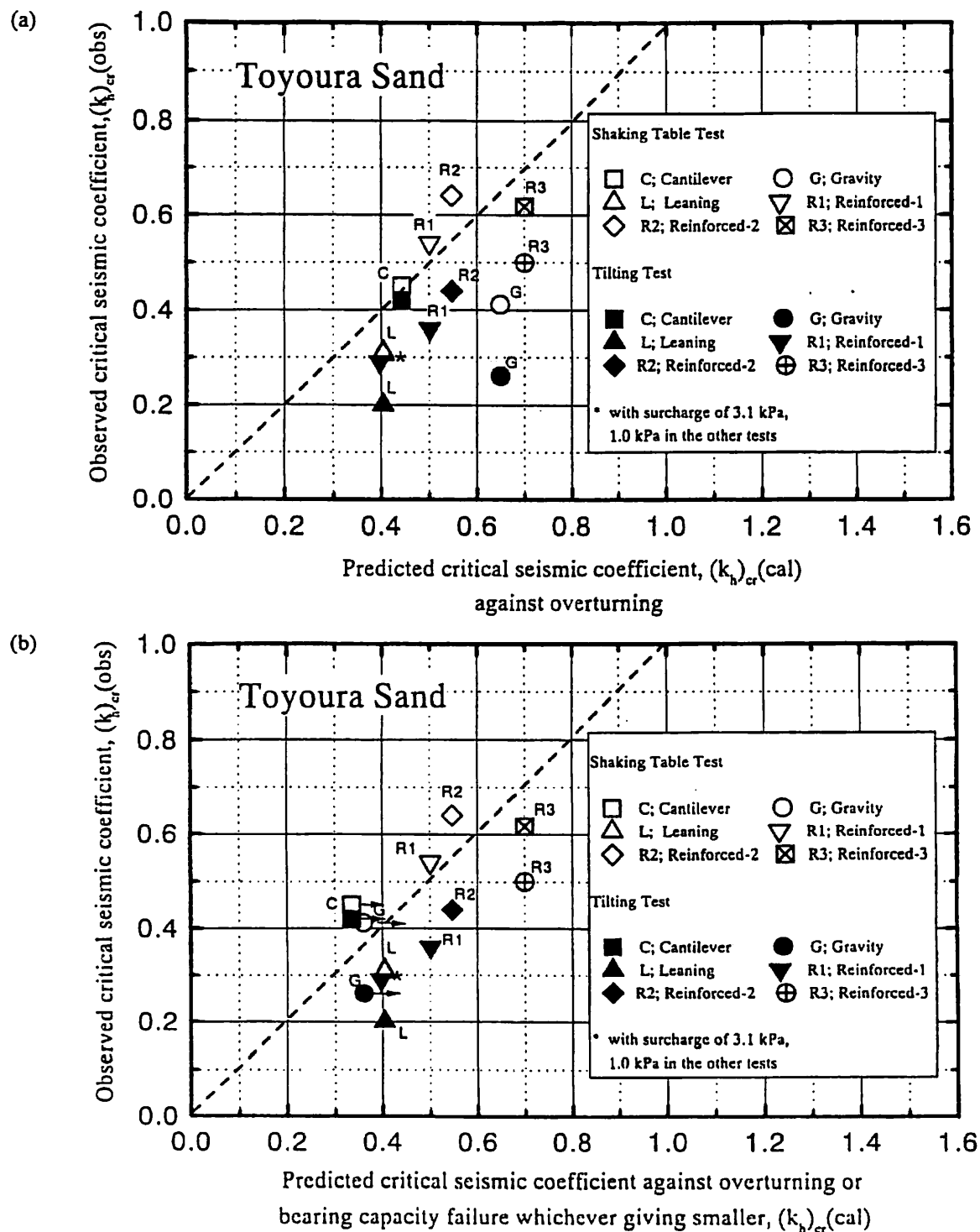


Fig. 6.2 Comparison of observed critical seismic coefficients $(k_h)_{cr}(obs)$ with predicted values $(k_h)_{cr}(cal)$ from tilting and shaking table tests of model RWs (Koseki et al., 1997).

coefficients $(k_h)_{cr}(obs)$. For the GRS-RWs, the bearing capacity at the facing base has been taken into account for the data shown in Figs. 6.2a and 6.2b. In so doing, the ultimate failure of RW due to the bearing capacity failure

has not been considered, since the wall can maintain its stability even when the load acting at the bottom of the facing reaches the bearing capacity of the subsoil, as demonstrated by a large-scale shaking test on a model of

GRS-RW (Murata et al., 1994). Lower $(k_h)_{cr}(\text{cal})$ values were obtained for bearing capacity failure with the cantilever and gravity-type RWs. The bearing capacity was evaluated assuming the subsoil thickness be sufficient to cause boundary-free subsoil failure despite that the actual thickness of the Toyoura sand layer was only 20 cm. Therefore, the safety factors against bearing capacity failure may have been somehow under-estimated. In Fig. 6.3b, this infer is indicated by arrows directing right shown next the data points for the cantilever and gravity-type RWs. The following trends may be seen from Fig. 6.2b:

1) The base width is the same, equal to 23 cm, among the gravity-type and cantilever RWs and the GRS-RW type 1 (see Fig. 4.7). The base width is 18 cm with the leaning-type RW, whereas the width between the top of the back face and the toe of the base is wider, equal to 33 cm. Despite the above, in the tilting tests, the GRS-RW type 1 and the cantilever RW have larger values of $(k_h)_{cr}(\text{obs})$ than the leaning-type and gravity-type RWs. In the shaking table tests, the GRS-RW type 1 is noticeably more stable than the others. This results are in a broad sense consistent with the full-scale field behaviour as shown in Fig. 6.1, suggesting a relatively high seismic stability of GRS-RWs having a FHR facing.

2) In the tilting tests, the ratio $(k_h)_{cr}(\text{obs})/(k_h)_{cr}(\text{cal})$ is generally lower than unity (except for the cantilever RW). This result suggests that the conventional pseudo-static approaches using peak plane strain soil strength obtained when the σ_1 direction is normal to the bedding plane direction over-estimate the stability of RW.

3) In the shaking table tests; the ratios $(k_h)_{cr}(\text{obs})/(k_h)_{cr}(\text{cal})$ are generally larger than unity, except for the leaning type RW, and different among the different RWs. This fact corresponds to; a) the observation in Fig 4.8 that in the shaking table tests, at the same $(k_h)_{cr}$, the failure plane angles ζ_r observed in the unreinforced backfill are generally larger than those predicted by the original M-O method using ϕ_{peak} ; and b) that in the shaking table tests, the ultimate failure of RW took place at k_h noticeably larger than the value where the active failure started in the backfill, and the difference depended on the RW type. The difference can be considered to be due to the dynamic effects. It is to be noted that $(k_h)_{cr}(\text{cal})$ values that are smaller than those shown in Fig. 6.2a are obtained when evaluated by the modified pseudo-static methods proposed in this report, giving larger ratios $(k_h)_{cr}(\text{obs})/(k_h)_{cr}(\text{cal})$. In that case, larger dynamic effects are evaluated.

4) In the shaking table test results, the ratios $(k_h)_{cr}(\text{obs})/(k_h)_{cr}(\text{cal})$ (shown in Fig. 6.2b) for the GRS-RW type 1 is similar to that for the cantilever RW, marginally larger than that for the gravity-type RW, and noticeably larger than that for the leaning-type RW. This trend is similar to that of the difference at a given $(k_h)_{cr}(\text{obs})$ value

between the measured value of ζ_r and that predicted by the original M-O method using ϕ_{peak} (shown in Fig. 4.8). The shaking table test results shown in Fig. 6.2 are, in a broad sense, consistent with the field full-scale behaviour of several representative types of RW which experienced extra-ordinary high seismic loads during the Hyogo-ken-nambu Earthquake (see Fig. 6.1). These results also suggest that the design values $(k_h)_{\text{design}}$ to be used in the pseudo-static analysis should be different, being smaller in the order of i) GRS-RWs having a FHR facing, ii) RC RWs, and iii) leaning and gravity-type RWs.

5) In the shaking table tests, the value of $(k_h)_{cr}(\text{obs})$ is largest for the GRS-RW type 2 having a couple of long reinforcement layers at high levels in the backfill. As seen from Fig. 4.7a, in this model, multiple failure planes developed; the one numbered 1, which was steepest, developed first from the heel of the backfill zone reinforced with short reinforcement layers and stopped somewhere below the lowest longer reinforcement layers; then, the other two numbered 2 and 3 developed, which were inclined much more horizontally, and developed up to the crest of the backfill. On the other hand, the value of $(k_h)_{cr}(\text{obs})$ is marginally smaller for the GRS-RW type 3 having the moderately long same-length reinforcement layers than Reinforced type 2, while the total amount of reinforcement was similar. When reconstructing existing slopes to vertical GRS-RWs, the use of relatively short reinforcements is preferred, because the amount of slope excavation can be minimized. Based on the test result described above, using several long reinforcement layers at high levels as the model Reinforced type 2 can be recommended to effectively increase the seismic stability of GRS-RWs having a FHR facing, compared with the GRS-RW type 1.

6) In the shaking table tests, after the first active failure occurred in the backfill, the k_h value could increase to a higher level until the ultimate failure of RW took place, exhibiting larger positive net dynamic effects, in the order i), ii) and iii) listed in the term 4). It seems that the modified M-O method and the modified TW method are more relevant for aseismic design of RWs exhibiting larger positive net dynamic effects when subjected to high seismic loads.

6.2 Dynamic effects

Different ratios of "design k_h "/(PGA/g) have been proposed for different types of foundation structures and RWs, which include the following:

i) By comparing the seismic behaviour of port and harbor gravity-type caissons placed on underwater mounds with their k_h values calculated following the design specification, Noda et al. (1975) obtained the following relationship;

$$(k_h)_{\text{critical}} = \text{PGA/g} \quad (\text{PGA} \leq 200 \text{ gals}) \quad (6.1a)$$

$(k_h)_{critical} = (1/3)(PGA/g)^{1/3}$ ($PGA \geq 200$ gals) (6.1b)
When following this relationship, $(k_h)_{critical} = 0.2, 0.246, 0.281, 0.309$ and 0.333 are obtained when $PGA/g = 0.2, 0.4, 0.6, 0.8$ and 1.0 .

- 2) Seed and Whitman (1970) proposed a value of 0.85 for retaining walls and bridge abutments against significant wall displacements.
- 3) The design manual guidelines for Terre Armee RWs of FHWA (FHWA 1990) employs the following relationship to evaluate the maximum wall acceleration coefficient α_m based on the maximum ground acceleration coefficient α_0 ;

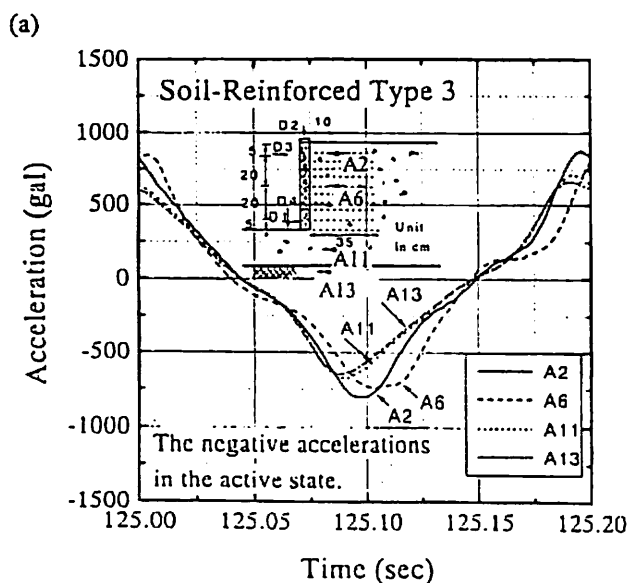
$$\alpha_m = (1.45 - \alpha_0) \alpha_0 \quad (6.2)$$

Note that the horizontal inertia force of the reinforced backfill is reduced by half to consider the effects of phase lag as mentioned in 3. When following this relationship, $(k_h)_{critical} = 0.25, 0.42, 0.51, 0.52$ and 0.45 are obtained when $PGA/g = 0.2, 0.4, 0.6, 0.8$ and 1.0 .

These ratios $(k_h)_{critical}/(PGA/g)$ are much lower than unity at high k_h values, which is seemingly due largely to the following three factors;

- a) underestimation of the soil strength used in evaluating the seismic stability of structure in terms of k_h to be compared with PGA/g (as in ordinary design procedures);
- b) simplifications in the design procedure leading to a safe side result such as that the passive pressure on the front face of the underground part of RW is ignored (but this could actually largely contribute to the seismic stability of actual RWs); and
- c) factors related to the so-called dynamic effects.

As seen from Figs. 4.8 and 6.2b, for the relatively



ductile RWs (i.e., the GRS-RWs), the value of $(k_h)_{cr(obs)}$ is larger than the corresponding value in the tilting test. This feature is likely due to that the net dynamic effects were positive. The following factors are important for the so-called dynamic effects on the seismic behaviour of RWs;

- 1) dynamic ductility of RW, which is the capability of the RW to survive "accelerations/g" exceeding the pseudo-static ultimate strength $(k_h)_{critical}$ by deforming without exhibiting seismic ultimate failure; this factor makes the structure more stable;
- 2) flexibility (or rigidity) of RW, resulting into the following three sub-factors;
 - a) phase difference in the lateral direction in the backfill, which usually increases with the RW flexibility, making also the RW more stable;
 - b) the coefficient β in Fig. Fig. 4.10a; for example, cantilever RC RWs, particularly those supported pile foundations, are rigid having a high value of β , resulting into higher seismic active pressure, while GRS-RWs are flexible having a low value of β , resulting into lower seismic active pressure; and
 - c) dynamic response of the structure, usually giving larger accelerations in the backfill than at the ground surface; this factor makes the RW less stable.

Related to the above factors 2a, 2b and 2c, in any shaking table test, the response acceleration, or dynamic amplification, is not uniform in both vertical and lateral directions, as typically seen from Fig. 6.3.

The difference in the $(k_h)_{critical}$ value between shaking table and tilting tests using the same model should become

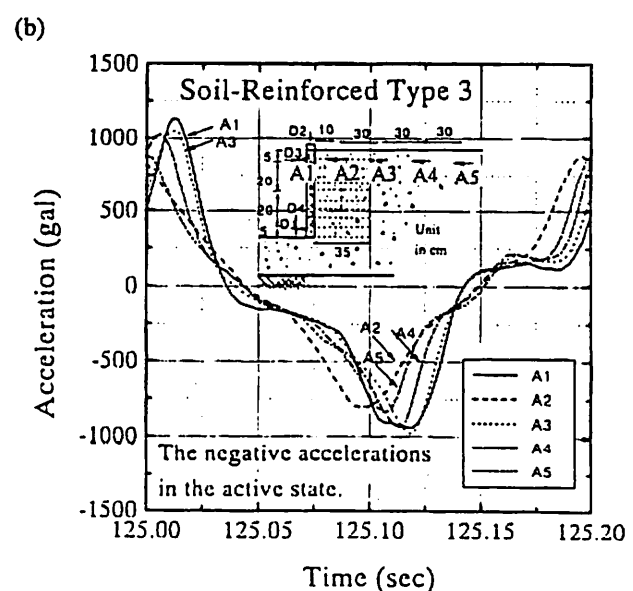


Fig. 6.3 Typical shaking table test of GRS-RW model ("Reinforced type 3") performed by the authors; a) comparison of response horizontal accelerations in the vertical (A2, A6, A11 and A13); and b) lateral (A1 to A5) directions, at input acceleration of about 600 gal.

larger when the shaking table test uses random cyclic loads with the value of $(k_h)_{critical}$ being defined as "the maximum table horizontal acceleration"/g at ultimate failure. For example, in the shaking table tests on the same type GRS-RW model having a discrete panel facing reported by Matsuo et al. (1997), the model wall failed by excessive outward deformation at a peak acceleration equal to 464 gals when the N-S component recorded at the Kobe Maritime Observatory during the 1995 Hyogo-ken-nambu Earthquake was used as the input random loads and at a single amplitude acceleration equal to 370 gals when twenty uniform sinusoidal waves were used as the input cyclic loads.

By using the cumulative damage theory, Murata et al. (1990) estimated the deformation of the GRS-RW having a FHR facing when subjected to a random cyclic loading based on the behaviour of the wall when subjected to uniform cyclic loadings at different acceleration levels. The procedure is similar to the one used for estimating the liquefaction strength of saturated sand when subjected to random seismic cyclic stresses based on the results obtained when subjected to uniform cyclic stresses (e.g., Tatsuoka et al., 1986). It was suggested by Murata et al. (1990) that for a given maximum input acceleration, the deformation of the model wall becomes much smaller when subjected to an irregular input motion than when subjected to a uniform motion, and the difference becomes larger as the number of cycles in the uniform motion increases, as the irregular motion becomes of more shock-type and as the RW becomes more dynamically ductile (i.e., factor 1 above).

6.3 Design k_h values

The design value of k_h , $(k_h)_{design}$, to be used in any pseudo-static analysis should reflect the fact that effects of the influencing factors, as listed in Table 6.1, are not perfectly, or are only poorly, reflected in the analysis. Therefore, the proper ratio of $(k_h)_{design}$ to the PGA/g of the design seismic load should depend on, at least, the following six factors;

- 1) the analysis method (e.g., the original M-O method and the conventional TW method using either peak or residual soil strength, or the modified M-O method and modified TW method using both peak and residual soil strengths);
- 2) the ratio of the design soil strength to the true operating soil strength;
- 3) positive effects of simplification used in the design (eg., no consideration of passive pressure on the front face of the underground part of facing);
- 4) the seismic ductility of RW, which depends on structure type (e.g., masonry, gravity, leaning, cantilever, or reinforced soil);- this factor is linked to the objective of aseismic design, which is different for Levels 1 and 2 seismic loads, as discussed before;

- 5) the seismic flexibility or rigidity of RW, which also depends on structure type and affects the dynamic response of RW; and
- 6) the global safety factor used in the aseismic design, which is usually 1.5 for RWs in Japan.

In the following, only design methods for Level 2 design seismic loads will be considered. Fig. 3.9 shows the values of $(k_h)_{cr}(cal)$ giving the safety factor equal to unity for several RWs which experienced extra-high seismic loads during the 1995 Hyogo-ken-nambu Earthquake. These $(k_h)_{cr}(cal)$ values were obtained by the conventional pseudo-static analyses (i.e., the original M-O method for the conventional type RWs and the conventional TW method for the GRS-RW) under the following two different conditions (see Table 3.3);

- A) the conventional design conditions using conservative soil strength (condition A; Table 3.1); and
- B) the conditions as close as the respective actual condition, while using peak soil strength (condition B; Table 3.2).

For all the data points, the estimated value of PGA/g is assumed to be 0.6 - 0.8 with an average of 0.7. As discussed before, to attain reasonable seismic stability, with a global safety factor equal to unity, the design value $(k_h)_{design}$ should be larger than the value of $(k_h)_{cr}(cal)$ for the collapsed types of RW, could be similar to the values of $(k_h)_{cr}(cal)$ for the moderately damaged but uncollapsed types of RW, and could be smaller than the values of $(k_h)_{cr}(cal)$ for the slightly damaged types of RW (note; for the cantilever RC RW at Tanata, this notion is valid only under the condition of the presence of the coffer dam in front of the wall, but it is not usual case and will not be discussed herein).

The following remarks are important:

- a) When based on the conventional pseudo-static analyses (i.e., the original M-O method for the conventional types of RW and the conventional TW method for GRS-RWs, both using conservative soil strength), the value of $(k_h)_{cr}(cal)$ was 0.10 for bearing capacity failure leading to overturning failure with the gravity type unreinforced concrete RW at Ishiyagawa and 0.09 for overturning failure with the leaning type unreinforced concrete RW at Sumiyoshi, both of which totally collapsed. These results suggest that for masonry RWs and leaning and gravity types unreinforced concrete RWs, even when based on the conventional pseudo-static analyses using conservative soil strength, the use of k_h equal to 0.1 - 0.2 is unconservative for Level 2 design seismic load. Obviously, the design value $(k_h)_{design}$ should be increased to a level much higher than 0.1 - 0.2, whereas it would be lower than, but a large fraction of, PGA/g of Level 2 seismic load (about 0.7 - 0.8).
- b) When based on the conventional pseudo-static analyses using peak soil strength, the value of $(k_h)_{cr}(cal)$ was 0.34

with the gravity type RW at Ishiyagawa and 0.48 for overturning failure with the leaning type RW at Sumiyoshi. Therefore, the use of $(k_h)_{design} = 0.1 - 0.2$ in the conventional pseudo-static analyses using peak soil strength is more unconservative than the current design method using conservative soil strength and therefore never be acceptable.

c) It is to be noted again that these values of $(k_h)_{cal}$ were back-calculated with an operating safety factor equal to unity. On the other hand, the allowable safety factor employed in the current aseismic design in Japan is typically 1.5. Part of the fraction 1.5 is considered to be assigned to uncertainties of load, and a lower allowance for uncertainties in the load is acceptable considering that the Level 2 seismic load is nearly the possible upper-bound design seismic load. Then, the suitable design value $(k_h)_{design}$ can be set to be, say, 0.9 times the value of $(k_h)_{cal}$ by which a given type of RW is moderately damaged but does not collapse with an operating safety factor equal to unity.

d) For the cantilever RC RWs, which were moderately damaged, when based on the conventional pseudo-static analyses using conservative soil strength, the values of $(k_h)_{cal}$ was 0.36 and 0.40 for bearing capacity failure with the two cantilever RC RWs at Ishiyagawa and 0.45 for bearing capacity failure with the cantilever RC RW at Rokko-michi. This result suggests that the use of $(k_h)_{design} = 0.1 - 0.2$ in the conventional pseudo-static analyses using conservative soil strength is also unconservative. However, the appropriate design value $(k_h)_{design}$ should be smaller than that for masonry RWs and leaning type and gravity type unreinforced concrete RWs. A value between $0.35 \times 0.9 \approx 0.3$ and $0.45 \times 0.9 \approx 0.4$ would be appropriate. Perhaps, this value is appropriate also for modern RC RWs supported by a pile foundation.

e) For the cantilever RC RWs, when based on the $(k_h)_{cal}(ob)$ values = 0.45 – 0.60 that were obtained by using peak soil strength, a value of $(k_h)_{design}$ is around $(0.45 - 0.60) \times 0.9 \approx 0.5$ would be appropriate.

f) For the Tanata GRS-RWs having a FHR facing, which was damaged only slightly, when based on the conventional pseudo-static analyses using conservative soil strength, the values of $(k_h)_{cal}$ was 0.36 for base sliding. It seems that the use of $(k_h)_{design}$ equal to 0.1 - 0.2 is unconservative, and a design value around $0.35 \times 0.9 = 0.3$ or less would be appropriate. When based on peak soil strength, a value of $(k_h)_{design}$ which is around $0.5 \times 0.9 = 0.45$ would be appropriate.

g) Summarizing the above, when based on the conventional pseudo-static analyses using conservative soil strength, $(k_h)_{design}$ equal to 0.4, 0.35 and 0.3 would be appropriate for, respectively, a) masonry RWs and leaning

type and gravity type RWs, b) properly designed and constructed RC cantilever RWs and c) GRS-RWs having a FHR facing. This proposed classification is supported by the shaking table model test results shown in Figs. 4.8 and 6.2b.

h) If the conventional pseudo-static analyses using peak soil strength is employed, the design value $(k_h)_{design}$ should be larger than those shown above; $(k_h)_{design} = 0.55, 0.50$ and 0.45 would be appropriate for, respectively, a) masonry, leaning type and gravity type RWs, b) properly designed and constructed RC cantilever RW and c) GRS-RWs having a FHR facing.

i) When based on the modified pseudo-static approach proposed in this report, the $(k_h)_{design}$ value would become higher than those used with the conventional pseudo-static analyses using conservative soil strength, becoming closer to the Level 2 PGA/g value (about 0.7). Considering that the failure mechanism can be better simulated, the use of the modified pseudo-static approach can be suggested for the aseismic design of GRS-RWs, particularly those having a FHR facing with relatively short reinforcement.

Based on the above and others, Fig. 6.4 was prepared. The design values $(k_h)_{design}$ which are tentatively proposed for Level 2 seismic loads, are indicated by the three inclined lines, which are respectively for a) GRS-RWs having a FHR facing; b) cantilever RC RWs; and c) masonry, gravity and leaning types of RWs. Along each line, the value of $(k_h)_{design}$ becomes smaller in the order of; a) the original M-O method and the conventional TW method using conservative soil strength; b) the modified M-O method and TW method using both peak and conservative soil strengths; and c) the original M-O method and the conventional TW method using peak soil strength.

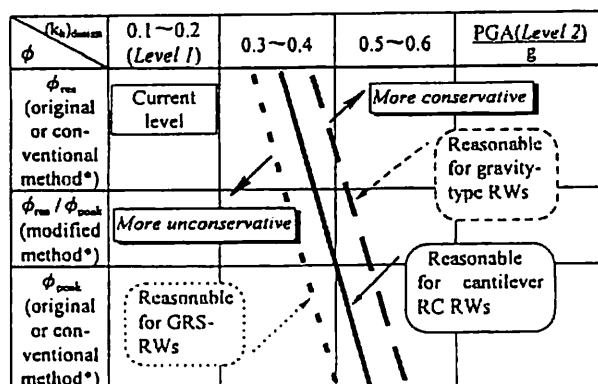
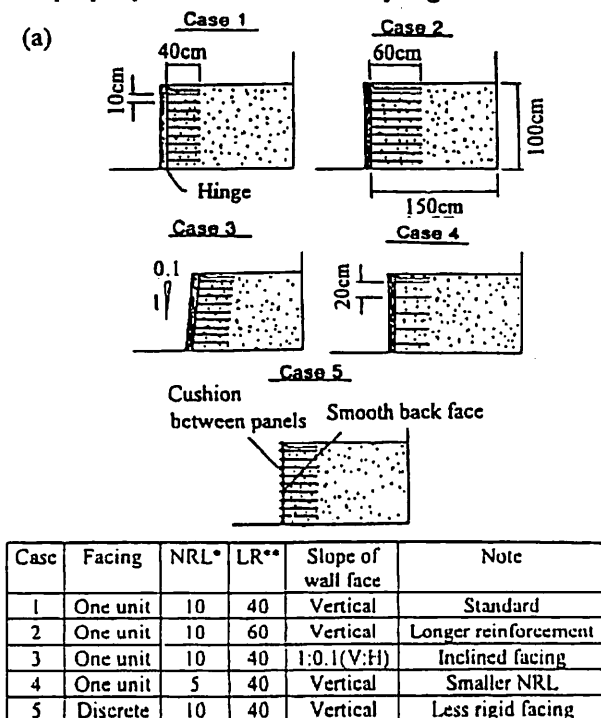


Fig. 6.4 Interrelations between seismic load (in terms of k_h or PGA/g), analysis method, structure type and seismic behaviour for Level 2 design load (tentative proposal).

6.4 Other important issues

Effects of reinforcement length: As discussed before, in the shaking table model tests described in Figs. 4.8 and 6.2, the GRS-RW having relatively long reinforcement (Reinforced type 3) was more stable than the GRS-RW having relatively short reinforcement (Reinforced type 1). In addition, the failure acceleration of the GRS-RW increased from 530 gals to 650 gals for over-turning failure by extending only a couple of top reinforcement layers (i.e., Reinforced type 2). Also in the shaking table tests on 100 cm-high grid-reinforced sand RW models performed by Murata, et al. (1990, 1992) (Fig. 6.5), under otherwise the same conditions, the GRS-RW model having longer reinforcement (case 2) was more stable than that having shorter reinforcement (case 1). This increase in the stability was attained by preventing the active failure plane starting from the heel of the reinforced zone to develop up to the backfill crest.

These results suggest that a shear band or failure plane is difficult to develop crossing reinforcement. Therefore, it is not relevant to always assume a single wedge to develop in reinforced backfill as in the unreinforced backfill. In particular, when based on the original M-O method using conservative soil strength assuming a single wedge, a very deep and largely inclined failure plane is predicted at a high k_s (see Fig. 5.5a); in that case, only one or two layers of short reinforcement can intersect with this failure plane, which may result into a design using long reinforcement layers from the bottom level. The modified TW method can properly evaluate the relatively high seismic stability



* NRL: Number of reinforcement layers

** LR: Length of reinforcement (in mm).

of the GRS-RW having short reinforcement at lower levels in the backfill.

On the other hand, in the shaking table model tests on 100 cm-high models of vertical GRS-RWs having a discrete panel facing with reinforcement layers truncated to the same length performed by Matsuo et al. (1997) (see Fig. 4.13), the failure acceleration increased from 370 gals to 575 gals by increasing the length of reinforcement from $L/H = 0.4$ to 0.7 under otherwise the same testing conditions. This test result is consistent with the shaking test results described above.

Effects of facing rigidity: The following trends of behaviour have been observed in the shaking table model tests of GRS-RWs with sand backfill (described so far in this report):

a) When the reinforcement was relatively short, such as $L/H = 0.4$, with a FHR facing, the predominant failure mode is overturning (Matsuo et al., 1997; Koseki et al., 1997).

b) In the tests on a 100 cm-high grid-reinforced sand model wall performed by Matsuo et al. (1997), under otherwise the same model configurations, when the facing was of discrete panels, the predominant failure mode was sliding with a failure plane passing inside the reinforced zone, resulting into a bulging deformation of the wall face.

c) In the tests by Matsuo et al. (1997), the effect of facing rigidity on the failure acceleration was small; the failure acceleration was 370 gals for a GRS-RW model having a discrete panel facing and 397 gals for a GRS-RW model having a FHR facing. It seems that this small difference

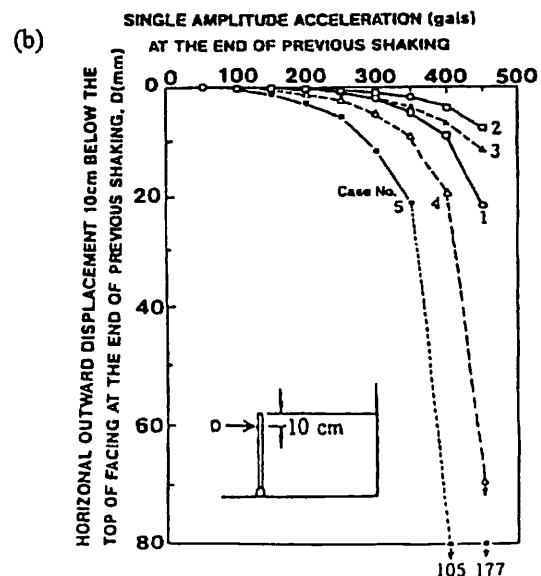


Fig. 6.5 Shaking table tests of GRS-RW models by Murata et al. (1992); a) test configuration; and b) relationships between table horizontal acceleration and outward displacement of wall.

resulted from that the stability of the GRS-RW having a FHR facing was relatively low. This was due likely to; a) relatively small pull-out resistance of the grid reinforcements resulting from; b) relatively short reinforcement length, $L = 0.4H$, with a relatively large vertical spacing S_v of reinforcement layers, 20 cm or $S_v/H = 0.2$; and c) a low density of the backfill ($D_r = 60\%$). On the other hand, in the shaking table tests presented in Fig. 6.5, under otherwise the same conditions, the GRS-RW model having a FHR facing (case 1) was much more stable than that having a discrete panel facing (case 5), despite that the ratio of the reinforcement length to the wall height was $L/H = 0.4$ as the tests by Matsuo et al. (1997). In these tests, the pull-out strength of grid was sufficiently large resulting from a small vertical grid spacing of 10 cm and a high density of the backfill ($D_r = 94\%$). Similar positive effects of using a FHR facing has been observed in the model tests reported by Bathurst and Alfaro (1996), in which the pull-out resistance of geogrid was large enough. It is likely, therefore, that the effects of facing rigidity become more important as the pull-out strength of reinforcement becomes larger; a) by preventing the occurrence of sliding failure having a failure plane passing inside the reinforced zone and appearing at an intermediate height at the wall face; and b) by confining better the backfill adjacent to the facing.

Effects of vertical acceleration (or k_v): Fig. 6.6 shows the plot of the combination of peak horizontal and vertical components of acceleration obtained from the time histories of acceleration recorded on the ground surface at Kobe Marine Meteorological Observation Station during the 1995 Hyogo-ken-nambu Earthquake. Table 6.2 shows the results of stability analysis of a typical GRS-RW having a FHR facing (see Fig. 2.2a) obtained by the conventional TW method using $\phi = 41^\circ$ for the backfill. It may be seen that the safety factor for the worst combination with the largest ratio of the outward horizontal acceleration to the upward vertical acceleration along the envelop of the data points is lower by only 1 % than that obtained using only the peak horizontal acceleration. It can be concluded, therefore, that

differences in results between the pseudo-static analyses of reinforced soil structure having a cohesionless soil backfill with and without considering the effects of vertical seismic load components are usually very small. A similar conclusion has been obtained by Bathurst and Alfaro (1996). Therefore, when considering a high degree of uncertainty in other factors, it is not unreasonable not to use vertical component of seismic load in routine aseismic design of reinforced soil structures including GRS-RWs having a FHR facing.

Evaluation of seismic ductility of RW: This could be made in a very approximated way by the method introduced in Tatsuoka et al. (1996). In this method, the ductility is evaluated by the area between the curve showing the relationship between the safety factor F , and the tilting angle of RW and the horizontal axis implying $F_s = 0.0$. However, the ductility could be better evaluated by estimating the deformation and displacement of RW by the method proposed by Newmark (1965) or its modifications, or the equivalent energy method described below, or the cumulative damage method.

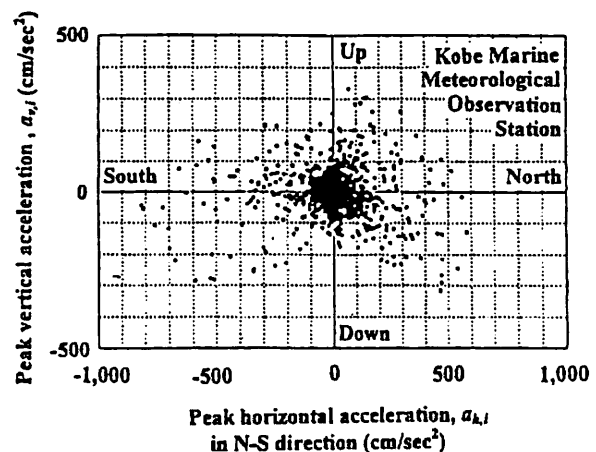


Fig. 6.6 Plot of the combination of horizontal and vertical components of acceleration obtained from the time histories of acceleration recorded on the ground surface at Kobe Marine Meteorological Observation Station during the 1995 Hyogo-ken-nambu Earthquake.

Table 6.2 Comparison of calculated critical seismic coefficients (k_h)_{cr}(cal) following the conditions listed in Table 3.2 for GRS-RW at Tanata with or without considering the effects of vertical acceleration.

Calculated critical seismic coefficients (k_h) _{cr} (cal)	Neglecting effects of vertical acceleration	Considering north component as outward horizontal acceleration and corresponding vertical acceleration	Considering south component as outward horizontal acceleration and corresponding vertical acceleration
Overtuning	0.597	0.591	0.626
Sliding	0.502	0.498	0.501

In the Newmark method, the displacement of a monolith during a seismic event is obtained as follows (Fig. 6.7):

1. The critical acceleration beyond which the monolith starts to slide is evaluated by a proper method such as pseudo-static analyses.
2. When the ground acceleration is in excess of the critical acceleration, the monolith is assumed to respond at a constant acceleration equal to the critical acceleration.
3. The residual displacement of the monolith relative to the ground is obtained by simply double-integrating difference between the accelerations of the monolith and the ground until the relative velocity of the monolith becomes zero upon the reversal of the ground acceleration direction.

Cai and Bathurst (1996a, b) and Ling et al. (1997) used this method to evaluate seismic residual lateral outward displacements of GRS-RW. On the other hand, only limited literature can be found on the method to evaluate the seismic overturning of retaining wall. Steedman and Zeng (1996) proposed a method to evaluate seismic rotation by rocking motion of large gravity walls placed on rigid foundations. Siddharthan et al. (1992) proposed a simple rigid plastic model for seismic tilting of rigid walls. Both methods consider both translation and tilting of the wall, and contact pressure on the bottom of the RW is evaluated by the method similar to the one used by the Japanese Railway Company (Haya et al., 1995 and RTRI, 1997). If the center of rotation of RW is assumed to be located near the toe of the wall, only a sliding mode of deformation is likely to occur, while when the center of rotation is located back the toe of the RW, a coupled (sliding and tilting) mode of displacement may result. It was also shown that the effects of the wall-soil friction angle δ_1 on the wall base be very large on the sliding displacement, while the effects of the wall-soil friction angle δ_2 on the wall back face be significant on the rotational displacement of the wall; a higher δ_2 results in a smaller rotational displacement.

The equivalent energy method (Fig. 6.8) has been proposed also by Newmark (1965) to estimate the seismic plastic deformation of a structure. Here, τ_y and u_y are the yielding stress and displacement, and τ_e and u_e are the elastic stress and displacement obtained without considering the effects of yielding. The total displacement u_m , which includes both the elastic and plastic components, is computed so that the elasto-plastic energy denoted by the total of the areas 1, 2 and 4 becomes equal to the elastic energy denoted by the total of the areas 1, 2 and 3. This method is popular in Seismic Structural Engineering to accommodate very high design seismic loads, such as Level 2, by allowing some plastic deformation of RC and steel structures. It is not certain whether this method is relevant also for soil structures, since they do not have an obvious yielding point. More

detailed discussion is beyond the scope of this short report.

FEM analyses: Even the failure of densely compacted unreinforced soil subjected to static loads is very difficult to be simulated by FEM, due mainly to the fact that proper simulation of strain localization into a shear band (or shear bands) and associated strain softening is an extremely complicated task (e.g., Tatsuoka et al., 1991). Complicated interaction between shear band deformation and reinforcement makes the failure analysis of reinforced soil more difficult (Kotake et al., 1997). Therefore, FEM analysis of the seismic failure of reinforced soil structure is still not a practical tool, and will not be discussed more.

Rupture strength of reinforcement for seismic loads;
Recent laboratory deformation and strength tests on

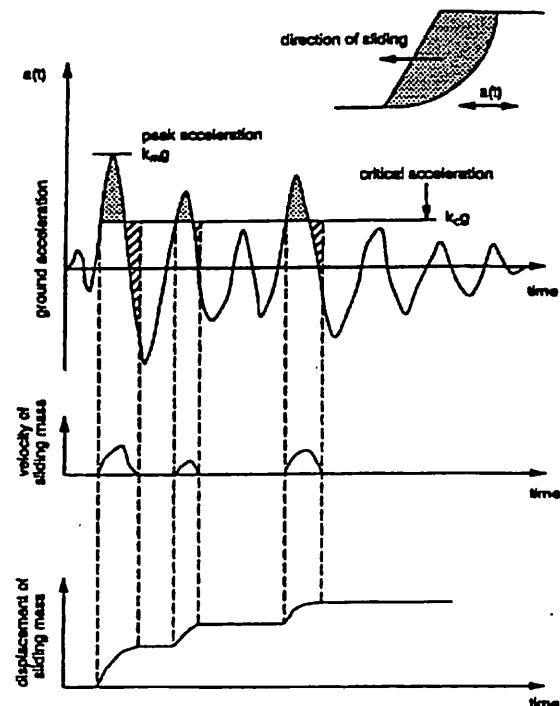


Fig. 6.7 Concept of Newmark's sliding block method (Cai and Bathurst, 1996a)

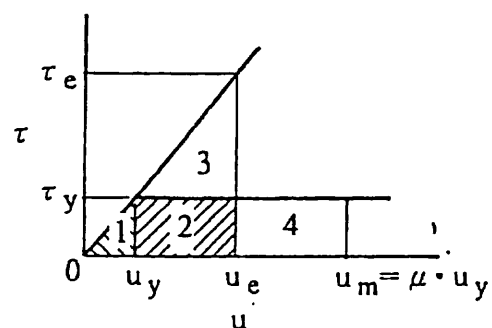


Fig. 6.8 Concept of equivalent energy method (Newmark, 1965)

geosynthetics showed that under the same strain rate, the strength after long-term creep is not smaller than that before creep (Bernardi and Paulson, 1997). This point is also discussed by Greenwood (1997). Therefore, no reduction factor is needed for the tensile strength of geosynthetic reinforcement to be used in seismic design compared with short-term design strength for static loads.

7. SUMMARY AND CONCLUSIONS

From the observations in the field, the model test results and the theoretical considerations summarized in this report, the following conclusions can be derived:

1. There exists a big gap between the design horizontal coefficients $(k_h)_{\text{design}}$ used in the current pseudo-static aseismic design approaches for retaining walls (RWs) and the peak ground accelerations (PGA) divided by the gravitational acceleration (g) experienced by a number of RWs during the 1995 Hyogo-ken-nambu Earthquake. This gap is due partly to; a) the use of conservative design soil strength; b) positive net dynamic effects that are not considered in the pseudo-static analyses; and c) the use of global safety factor larger than unity. At the same time, serious damage to a number of RWs during the earthquake shows that the current $(k_h)_{\text{design}}$ values should be increased appropriately to avoid such damage.
2. In both the field behaviour and the laboratory model tests, for the same safety factor evaluated by the pseudo-static approach, the seismic stability of GRS-RW having a FHR facing was marginally higher than that of cantilever RC RWs not supported by a pile foundation, and noticeably higher than that of leaning and gravity-type RWs not supported by a pile foundation.
3. The observations in both the field and the laboratory revealed that large apparent inconsistencies exist in the size of failure zone between the conventional pseudo-static analyses and the actual observations.
4. In the laboratory static tilting model tests, irrespective of RW type, a failure plane or a set of failure planes developed in the backfill associated with the active failure in the backfill, followed by the ultimate failure or collapse of RW only at a slightly larger tilting angle. On the other hand, in the laboratory shaking table model tests, the ultimate failure or collapse of RW occurred at a later stage associated with relative large deformations and displacements of RW occurring after the first active failure plane developed in the backfill. The difference was due to positive net dynamic effects, which were different among the different types of RW. Yet, it is likely that the first developed active failure mechanism controlled the ultimate failure of the RW (except for the GRS-RW having several top or all long reinforcement layers). Therefore, similarly to the pseudo-static approaches, the static tilting tests are not appropriate to evaluate such seismic stability of RW as observed in the field and the shaking table tests.
5. The soil strength along the failure plane can drop very rapidly with very small shear deformation from the peak value to the residual value. It is very likely, therefore, that the peak strength along the failure plane has dropped to the residual value at the moment of the ultimate failure or collapse of RW.
6. Based on the above observations 1~5, a modified pseudo-static approach can be proposed to evaluate the dynamic active earth pressure acting on; a) the back face of RW with unreinforced backfill; and b) the back face of the full-height rigid facing of GRS-RW. The modified approach predicts smaller dynamic earth pressure and smaller failure zones in the backfill than those predicted by the conventional pseudo-static approaches using conservative soil strength, which is usually similar to the residual strength. According to the modified pseudo-static approach, the use of short reinforcement layers can increase largely the seismic stability of GRS-RW, particularly at high seismic loads. This estimation is consistent with the field and laboratory observations.
7. The design horizontal seismic coefficient $(k_h)_{\text{design}}$ depends not only the PGA value of design seismic load, but also many other factors, among which; a) stability analysis method; b) design soil strength; c) simplification of wall configurations employed in the design; d) dynamic effects, among which the ductility and rigidity of RW and the frequency properties and randomness of seismic loads are important; and d) the global safety factor.
8. It is suggested that under otherwise the same conditions, the design value $(k_h)_{\text{design}}$ for well-designed and constructed GRS-RW having a FHR facing could be marginally smaller than that for masonry RWs and noticeably smaller than that for masonry RWs and leaning and gravity types RWs. When RWs are designed against Level 2 seismic loads by the conventional pseudo-static analysis using conservative soil strength, while using an allowable global safety factor equal to 1.5;
 - a) for masonry RWs and leaning and gravity types RWs; the use of $(k_h)_{\text{design}} = 0.1 - 0.2$ is unconservative, and $(k_h)_{\text{design}} = 0.40$ could be tentatively suggested;
 - b) for cantilever RC RWs; the use of $(k_h)_{\text{design}} = 0.1 - 0.2$ is unconservative, and $(k_h)_{\text{design}} = 0.35$ could be tentatively suggested; and
 - c) for GRS-RWs having a FHR facing; the use of $(k_h)_{\text{design}} = 0.1 - 0.2$ may be unconservative, and $(k_h)_{\text{design}} = 0.30$ could be tentatively suggested.
9. The use of several long reinforcement layers at high levels is effective to increase seismic stability of GRS-RWs.

8. ACKNOWLEDGMENTS

Funding for this study was provided by the Ministry of Education, Science, Sports and Culture, Japan. The authors wish to thank Messrs. S. Nishihara at Chuo Kaihatsu Co., K. Kojima at Railway Technical Research Institute, T. Tsutsumi at Public Works Research Institute, K. Hayano, T. Uchimura and T. Sato at University of Tokyo for their help in preparing the manuscript.

REFERENCES

- Bathurst, R.J. and Cai, Z. (1995) "Pseudo-Static Seismic Analysis of Geosynthetic-Reinforced Segmental Retaining Walls", *Geosynthetics International*, Vol. 2, No. 5, pp. 787-830.
- Bathurst, R.J. and Alfaro, M.C. (1996) "Review of Seismic Design, Analysis and Performance of Geosynthetic Reinforced Walls, Slopes and Embankments", *Earth Reinforcement*, (Ochiai et al., eds.), Balkema (in print).
- Bernardi, M. and Paulson, J. (1997), "Is creep a degradation phenomenon?", *Mechanically Stabilized Backfill* (Wu, J.T.H. eds.), Balkema, pp. 289-294.
- Bolton, M.D. and Steedman, R.S. (1985) "Modeling the Seismic Resistance of Retaining Structures", *Proc. 11th ICSMFE*, Vol. 4, pp. 1845-1848.
- Cai, Z. and Bathurst, R.J. (1996a) "Deterministic Sliding Block Methods for Estimating Seismic Displacements of Earth Structures", *Soil Dynamics and Earthquake Engineering* 15, Elsevier, pp. 255-268.
- Cai, Z. and Bathurst, R.J. (1996b) "Seismic-Induced Permanent Displacement of Geosynthetic-Reinforced Segmental Retaining Walls", *Canadian Geotechnical Journal*, Vol. 33, pp. 937-955.
- Collin, J.G., Chouery-Curtis, V.E. and Berg, R.R. (1992) "Field Observation of Reinforced Soil Structures under Seismic Loading", *Earth Reinforcement Practice* (Ochiai et al., eds), Balkema, Vol. 1, pp. 223-228.
- Federal Highway Administration (1990) "Reinforced Soil Structures Volume I. Design and Construction Guidelines", Publication No. FHWA-RD-89-043, p.100.
- Fukuda, N., Tajiri, N., Yamanouchi, T., Sakai, N. and Shintani, H. (1994) "Applicability of Seismic Design Methods to Geogrid Reinforced Embankment", *Proc. 5th International Conference on Geotextiles, Geomembranes and Related Products*, Singapore, pp. 533-536.
- Greco, V. R. (1997) "Stability of Retaining Walls against Overturning", *Journal of Geotechnical and Geoenvironmental Engineering*, Vol. 123, No. 8, pp. 778-780.
- Greenwood, J.H. (1997) "Designing to Residual Strength of Geosynthetics Instead of Stress-Rupture", *Geosynthetics International*, Vol. 4, No. 1, pp. 1-10.
- Haya, H., Sawada, R. and Nishimura, A. (1995) "Loading and Vibration Tests for Spread Foundation", *Proc. of 10th Asian Regional Conference on SMFE*, Vol. 1, pp. 203-206.
- Horii, K., Kishida, H., Tateyama, M. and Tatsuoka, F. (1994) "Computerized Design Method for Geosynthetic-Reinforced Soil Retaining Walls for Railway Embankments", *Recent Case Histories of Permanent Geosynthetic-Reinforced Soil Retaining Walls* (Tatsuoka and Leshchinsky, eds.), Balkema, pp. 205-218.
- Ichihara, M. and Matsuzawa, H. (1973) "Earth Pressure during Earthquake", *Soils and Foundations*, Vol. 13, No. 4, pp. 75-86.
- Japan Society of Civil Engineers (1996) "Proposal on Earthquake Resistance for Civil Engineering Structures (Special Task Committee of Earthquake Resistance of Civil Engineering Structures)", *The 1995 Hyogoken-nanbu Earthquake - Investigation into Damage to Civil Engineering Structures*, Committee of Earthquake Engineering, Japan Society of Civil Engineers, pp. 297-306.
- Jewell, R.A., Paine, N. and Woods, R.I. (1984) "Design Methods for Steep Reinforced Embankments", *Polymer Grid Reinforcement*, McGown et al. (eds.), Thomas Telford, pp. 70-81.
- Jewell, R.A. (1991) "Application of Revised Design Charts for Steep Reinforced Slope", *Geotextiles and Geomembranes*, Vol. 10, pp. 203-233.
- Koseki, J., Tateyama, M., Tatsuoka, F. and Horii, K. (1996) "Back Analyses of Soil Retaining Walls for Railway Embankments Damaged by the 1995 Hyogoken-Nanbu Earthquake", *The 1995 Hyogoken-nanbu Earthquake - Investigation into Damage to Civil Engineering Structures*, Committee of Earthquake Engineering, Japan Society of Civil Engineers, pp. 101-114.
- Koseki, J., Munaf, Y., Tatsuoka, F., Tateyama, M., Kojima, K. and Sato, T. (1997) "Shaking Table and Tilting Tests of Geosynthetic-Reinforced Soil Retaining Wall and Conventional Type Retaining Wall Models", *Geosynthetics International* (submitted).
- Koseki, J., Tatsuoka, F., Munaf, Y., Tateyama, M., and Kojima, K. (1997a) "A modified procedure to evaluate active earth pressure at high seismic loads" *Soils and Foundations* (submitted).
- Kotake, N., Tanaka, T., Tatsuoka, F. and Yamauchi, H. (1997), "Numerical simulation of strain localization and failure in reinforced soil," *Proc. Int. Conf. on Deformation and Progressive Failure in Geomechanics*, IS Nagoya '97 (Asaoka, Adachi and Oka eds.), Pergamon Press, pp. 247-252.
- Leshchinsky, D., Ling, H.I. and Hanks, G. (1995) "Unified Design Approach to Geosynthetic Reinforced Slopes and Segmental Walls", *Geosynthetics International*, Vol. 2, No. 5, pp. 845-881.
- Ling, H. I. and Leshchinsky, D. and Perry, E.B. (1997) "Seismic Design and Performance of Geosynthetic-Reinforced Soil Structures", *Geotechnique* (accepted)

- for publication).
- Matsuo, O., Tsutsumi, T. and Saito, Y. (1997) "Shaking Table Tests and Analysis of Geosynthetic-Reinforced Soil Retaining Walls", *Geosynthetics International* (submitted).
- Mononobe, N. and Matsuo, H. (1929) "On Determination of Earth Pressure during Earthquake", *Proc. World Engineering Congress*, Tokyo, Vol. 9, pp. 177-185.
- Munaf, Y., Koseki, J., Tateyama, M., Kojima, K. and Sato, T. (1997) "Model Tests on Seismic Performance of Retaining Walls", *Bulletin of Earthquake Resistant Structure Research Center*, No. 30, pp. 3-18.
- Murata, O., Tateyama, M., and Tatsuoka, F. (1990) "Shaking Table Tests on Sand Backfill Reinforced with Short Geogrid-Reinforcement with Various Types of Facings", *Proc. of 25th Japan National Conference on Soil Mechanics and Foundation Engineering*, pp. 2019-2022 (in Japanese).
- Murata, O., Tateyama, M., and Tatsuoka, F. (1992) "Loading Tests of Geosynthetic-Reinforced Soil Retaining Walls and Their Stability Analysis", *Earth Reinforcement Practice*, (Ochiai et al., eds.), Balkema, Vol. 1, pp. 385-390.
- Murata, O., Tateyama, M., and Tatsuoka, F. (1994) "Shaking Table Tests on a Large Geosynthetic-reinforced Soil Retaining Wall Model", *Recent Case Histories of Permanent Geosynthetic-reinforced Soil Retaining Walls*, (Tatsuoka and Leshchinsky eds.), Balkema, Vol. 1, pp. 259-264.
- Newmark, N.M. (1965) "Effects of Earthquakes on Dams and Embankments", *Geotechnique*, Vol. 15, No. 2, pp. 139-159.
- Noda, S., Uwabe, T. and Chiba, T. (1975) "Relation between Seismic Coefficient and Ground Acceleration for Gravity Quay Wall", *Report of Port and Harbour Research Institute*, Vol. 14, No. 4, pp. 67-111 (in Japanese).
- Okabe, S. (1924) "General Theory on Earth Pressure and Seismic Stability of Retaining Wall and Dam", *Journal of Japan Society of Civil Engineers*, Vol. 10, No. 6, pp. 1277-1323.
- Public Works Research Institute (1992) "Design and Construction Manual of Geotextile Reinforced Soil Structures", *Research Report of Public Works Research Institute*, No. 3117, 404 p. (in Japanese).
- Railway Technical Research Institute (1997): "Design Standard for Railway Foundations/Soil Retaining Structures", pp. 132-135 (in Japanese).
- Seed, H.B. and Whitman, R.V. (1970) "Design of Earth Retaining Structures for Dynamic Loads", *ASCE Specialty Conference on Lateral Stresses in the Ground and Design of Earth Retaining Structures*, pp. 103-147.
- Siddharthan, R., Ara, S., and Norris, G.M. (1992) "Simple Rigid Plastic Model for Seismic Tilting of Rigid Walls", *Journal of Structural Engineering*, Vol. 118, No. 2, pp. 469-487.
- Steedman, R.S. and Zeng, X. (1996) "Rotation of Large Gravity Walls on Rigid Foundations under Seismic Loading", *Analysis and Design of Retaining Structures against Earthquakes*, Geotechnical Special Publication No. 60, ASCE, pp.38-56.
- Tateyama, M. (1997) "Study on the Construction Methods for Reinforced Soil Retaining Walls using Facing Rigidity", Doctoral thesis, University of Tokyo, pp. 28-42 (in Japanese).
- Tatsuoka, F., Maeda, S., Ochi, K. and Fujii, S. (1986) "Prediction of undrained strength of sand subjected to irregular loading," *Soils and Foundations*, Vol.26, No.2, pp.73-90.
- Tatsuoka, F., Okahara, M., Tanaka, T., Tani, K., Morimoto, T. and Siddiquee, M. S. A. (1991) "Progressive Failure and Particle Size Effect in Bearing Capacity of a Footing on Sand", *Geotechnical Engineering Congress 1991*, Mclean, F., Campbell, D. and Harris, D., Editors, ASCE, Geotechnical Special Publication No.27, Vol. 2, pp.788-802.
- Tatsuoka, F., Koseki, J. and Tateyama, M. (1996) "Performance of Reinforced Soil Structures during the 1995 Hyogo-ken Nanbu Earthquake", *Earth Reinforcement*, (Ochiai et al., eds.), Balkema (in print).
- White, D.M. and Holtz, R.D. (1996) "Performance of Geosynthetic-Reinforced Slopes and Walls during the Northridge, California Earthquake of January 17, 1994", *Earth Reinforcement*, (Ochiai et al., eds.), Balkema (in print).
- Yamada, S., Masuda, T., Sato, T., Yamaguchi, I. and Tatsuoka, F. (1996) "Sand Behavior in Plane Strain Compression Test", *Proc. of 31st Japan National Conference on Geotechnical Engineering*, pp. 683-684 (in Japanese).
- Yoshida, T., Tatsuoka, F., Siddiquee, M. S. A., Kamegai, Y. and Park, C. S. (1994) "Shear Banding in Sands Observed in Plane Strain Compression", *Localisation and Bifurcation Theory for Soils and Rocks*, Chambon, Desrue and Vardoulakis (eds.), Balkema, pp. 165-179.
- Yoshida, T. and Tatsuoka, F. (1997) "Deformation Property of Shear Band in Sand Subjected to Plane Strain Compression and its Relation to Particle Characteristics", *Proc. of 14th ICSMFE*, Hamburg, Vol. 1, pp.237-240.